Dissipative properties of Runge-Kutta schemes with upwind spatial approximation for the Euler equations

Marie-Helene Lallemand

INRIA

UNITE DE RECHERCHE
INRIA-SOPHIA ANTIPOLIS

Institut National
de Recherche
en Informatique
et en Automatique

Domaine de Voluceau
Rocquencourt
BP 105
78153 Le Chesnay Cedex
France
Tél (1) 39 63 55 11

Rapports de Recherche

N° 1173

Programme 7
Calcul Scientifique,
Logiciels Numériques et Ingénierie Assistée

DISSIPATIVE PROPERTIES OF RUNGE-KUTTA SCHEMES WITH UPWIND SPATIAL APPROXIMATION FOR THE EULER EQUATIONS

Marie-Hélène LALLEMAND

Mars 1990

RR-1173

DISSIPATIVE PROPERTIES OF RUNGE–KUTTA SCHEMES WITH UPWIND SPATIAL APPROXIMATION FOR THE EULER EQUATIONS

PROPRIETES DISSIPATIVES DES SCHEMAS DE RUNGE–KUTTA A 4 PAS EN APPROXIMATION DECENTREE APPLICATION A LA RESOLUTION DES EQUATIONS D'EULER

Marie–Hélène Lallemand

Department of Mathematics
1200 Larimer Street
Campus Box 170
Denver Colorado 80204–5300 (USA)

ABSTRACT

We present in this paper how to construct a 4–stage Runge–Kutta method when the spatial approximation is a MUSCL–type upwind scheme for the solution of the two–dimensional Euler equations.

A theorical study is first conducted in the one–dimensional linear case, and then extended to the two–dimensional case where the equations are solved by multigrid techniques over unstructured finite element meshes.

A few numerical experiments are presented, demonstrating the validity of the theoretical results.

RESUME

On présente ici une méthode de construction d'un schéma de Runge–Kutta à 4 pas combiné à une approximation spatiale décentrée de type MUSCL pour la résolution des équations d'Euler en 2 dimensions.

Une étude théorique est d'abord menée dans le cas monodimensionnel et linéaire puis étendue en 2 dimensions pour des techniques multigrilles utilisant des maillages en éléments finis non structurés.

Quelques résultats numériques sont présentés, mettant en évidence la validité de cette étude.

Contents

1 MULTIGRID TECHNIQUE 2
- 1.1 The basic algorithm . . . 2
- 1.2 The "Full Multigrid" algorithm . . . 4

2 1–D STABILITY ANALYSIS 5
- 2.1 The 1–D Conservation law model . . . 5
  - 2.1.1 Finite Volume approximation . . . 5
  - 2.1.2 The time scheme . . . 6
  - 2.1.3 Spatial approximation schemes . . . 7
  - 2.1.4 Local Fourier mode analysis . . . 11
- 2.2 Optimization of the RK4 scheme . . . 12
  - 2.2.1 1–grid case . . . 12

3 2–D EXTENSION 22
- 3.1 First order accurate upwind scheme . . . 22
- 3.2 Second–order upwind scheme . . . 23
- 3.3 Stability condition . . . 24
- 3.4 2–D extension . . . 25

4 NUMERICAL RESULTS 32

5 APPENDIX 42

References 45

INTRODUCTION

We study in this report the dissipative properties of a class of linearized 4-steps Runge–Kutta schemes (RK4) and we are interested in upwind spatial approximations applied to hyperbolic problems.

The upwind schemes which are studied here are first or second order accurate in space.

The study is done in the scalar case, using the classical advection equation as a model equation, and we are interested in the behavior of the amplification factor, obtained from Fourier analysis; this work can be related to others done by Jameson in [8, 9, 10] and E. Turkel and B. van Leer in [16].

What is proposed here, is to adjust the parameters defining a variant of the classical RK4 method to achieve the best dissipative properties at the highest frequency. The objective is to construct an efficient smoother, basic ingredient of a multigrid algorithm, when upwind spatial discretization is applied to steady Euler computations.

Moreover, the present study has the originality to be concerned with Finite Element discretizations. This is a part of many works that were already (and is still being) done in order to build Finite Element multigrid methods for *unstructured* meshes. By *unstructured*, we mean that the number of elements having a common node is not a constant thoughout the computational domain. These elements are triangles in 2–D, tetrahedra in 3–D. The nodes in the mesh correspond to the vertices of these elements and the approximate solution is computed in these nodes.

Employing unstructured Finite Element discretizations is indeed convenient in the case of complex geometries that often appear in the industrial computations. They also more easily allow the use of mesh adaption techniques (refinement/movement) [13, 1, 14, 15].

Runge–Kutta methods are also very simple to implement and require a very low memory storage and cost. Moreover, they permit the use of a larger choice of spatial approximation methods.

Thus, the present study can be generalized to other types of spatial approximation than upwind methods and complete in some sense the study done by A. Jameson in the multigrid context [10].

The main principles of the multigrid algorithm are briefly recalled in section 2.

In section 3, we are studying the combination of a RK4 scheme with an upwind first– or second–order accurate spatial approximation in the 1–D linear multigrid context. As advised by A. Brandt in [3], we do a *local Fourier mode analysis* to evaluate the amplification (or smoothing) factor. This analysis allows us to define some criteria that define the optimal parameters (RK4 coefficients and the Courant number), to be chosen. Notice that, in the upwind spatial approximation context, there is no direct control of the viscosity since it is a

part of differencing. Then, the optimization of the other parameters is very important.

In section 4, we investigate a 2–D extension of the previous study. That is done by defining new criteria that are essentially related to the geometry.

Some numerical results are presented in section 5 in order to illustrate and validate this new study.

1 MULTIGRID TECHNIQUE

Because we want to solve the 2–D Euler equations that are *non–linear*, the basic multigrid algorithm we use is of the FAS *Full Approximation Scheme* [3] type and is non fundamentally different from those used by Jameson in [8] except that we deal with upwind spatial Finite Element discretization context.

One can find more details about the two multigrid algorithms used in [11, 12]. There, we just recall their main lines.

1.1 The basic algorithm

The basic iterative method (or solver) we use is a RK4 scheme adapted to upwind spatial approximations. We are also concerned with the Multi–Triangulation (MT) scheme in which the different grids are nested triangulations (see [11, 12]).

The FAS multigrid algorithm is an adaptation of the classical one (usually defined for solving linear systems) when the discretized operators are non linear.

The main principle of the multigrid method is to compute an approximation of the fine–grid solution correction on coarser levels. Each *iteration*, usually called *cycle*, corresponds here to the change of the fine–grid solution between time level t_n to time level t_{n+1}.

Let $\{G_k\}_{1\leq k\leq N}$ be a nested set of grids, $N > 1$, where G_1 is the finest grid. We denote F_k the non linear (with respect to the unknown W_k) discretized operator defined on G_k, $k = 1, \ldots, N$. The discrete non linear steady state problem that we have to solve on G_1 can be written as follows

$$F_1(W_1) = s_1 \ , \tag{1}$$

where s_1 denotes the right hand side which can be zero.

If $W_1^{(0)} \equiv W_1^n$ is the initial guess given at time t_n, we can improve the approximate solution $\overline{W}_1$ of problem (1) by applying ν_1 iterations of the basic non linear pseudo–unsteady state iterative method (that is RK4 here). This can be written as follows

$$\begin{array}{rl} W_1^{(l)} & = \mathcal{S}_1(W_1^{(l-1)}, s_1) \ , \quad l = 1, \ldots, \nu_1 \ , \\ \overline{W}_1 & = W_1^{(\nu_1)} \ . \end{array} \tag{2}$$

The iterative method $\mathcal{S}_1$ is non linear with respect to the initial iterate $W_1^{(0)}$, because of the non linearity of the spatial operator F_1; by pseudo-unsteady we mean that the exact steady solution of (1) can also be considered as a special solution of the following evolution problem

$$\frac{dW_1}{dt} + (F_1(W_1) - s_1) = 0 \ .$$

This will be made more precise when using a Runge–Kutta method in § 2.3.

Consider that $\overline{W}_1$ is sufficiently closed to the exact solution W_1^* of (1), i.e.

$$F_1(\overline{W}_1) - s_1 \simeq 0 \ ,$$

then $\overline{W}_1$ can be chosen to be the approximate solution W_1^{n+1} at time t_{n+1}.

Otherwise, we can notice that the correction of $\overline{W}_1$ on G_1 corresponds to the difference $C_1 = (W_1^* - \overline{W}_1)$, and

$$W_1^* = \overline{W}_1 + C_1 \ .$$

Thus, a better approximate solution can be obtained if C_1 can be evaluated. Because F_1 is non linear, we cannot obtain this correction directly ($F_1(W_1^* - \overline{W}_1) \neq F_1(W_1^*) - F_1(\overline{W}_1)$), but observing that

$$F_1(W_1^*) - F_1(\overline{W}_1) = s_1 - F_1(\overline{W}_1) \ , \tag{3}$$

we can compute it approximatively by solving the non linear system derived from (3) on a coarser grid G_2

$$\begin{array}{rcl} F_2(W_2) & = & F_2(W_2^{(0)}) + \mathbf{I}_{1,2}\left(s_1 - F_1(\overline{W}_1)\right) \ , \\ W_2^{(0)} & = & \mathbf{I}_{1,2}(\overline{W}_1) \ , \end{array} \tag{4}$$

where $\mathbf{I}_{1,2}$ is a (linear) restriction operator from G_1 to G_2. (4) can be rewritten in a form similar to (1)

$$\begin{array}{l} F_2(W_2) = s_2 \ , \\ s_2 = F_2(W_2^{(0)}) + \mathbf{I}_{1,2}\left(s_1 - F_1(\overline{W}_1)\right) \ . \end{array} \tag{5}$$

Let $\overline{W}_2$ be an approximate solution of (5), then this is an approximation of the *full corrected solution* $\overline{W}_1 + C_1 = W_1^*$ on G_2 ; the approximate correction of $\overline{W}_1$ on G_1 is thus obtained by

$$\mathcal{I}_{2,1}(\overline{W}_2 - W_2^{(0)}) = \mathcal{I}_{2,1}(\overline{W}_2 - \mathbf{I}_{1,2}(\overline{W}_1)) \approx W_1^* - \overline{W}_1 \ ,$$

$\mathcal{I}_{2,1}$ is a prolongation operator from G_2 to G_1. The new corrected value that approximates W_1^* on G_1 is

$$\overline{W}_1^* = \overline{W}_1 + \mathcal{I}_{2,1}(\overline{W}_2 - W_2^{(0)}) \ . \tag{6}$$

This new value can be kept to define the "solution" W_1^{n+1} at time t_{n+1}, and is a better approximate solution than $\overline{W}_1$, but it can also be improved by applying ν_2 iterations of the method defined by (2) with $W_1^{(0)} = \overline{W}_1^*$, and $\overline{W}_1 = W_1^{n+1}$.

The procedure given above is defined to be a 2–grid FAS iteration [3] also called *2–grid cycle* and denoted by $\mathbf{MG}_{FAS}(G_1, G_2)$.

It can easily be generalized to N grids by noticing that the approximate solution $\overline{W}_2$ can be obtained by applying μ cycles $\mathbf{MG}_{FAS}(G_2, G_3)$; the same is done for the problem related to grid G_3, and so on, down to the coarsest level N, where the approximate solution $\overline{W}_N$ can be computed by an iterative method similar to (2) (or any other simpler one) after applying ν_G iterations (in practice, $\nu_G = \nu_1 + \nu_2$).

The step of the previous algorithm defined by (4) and (6) is called *Coarse Grid Correction* (CGC).

The method defined in (2) is similar to a non linear relaxation method. It should have good smoothing properties if we want the problem to be well represented by the coarse–grid iterations. This requires that the high–frequency content of the error be damped by the relaxation.

When $\mu = 1$, the multigrid iteration is called *V–cycle*. When $\mu = 1$, $\nu_1 \geq 1$, $\nu_2 = 0$, it is called *"saw–tooth cycle"*, (see [12], chapter 1) because no relaxation is applied after the correction step, but only a direct transfer of the coarse–grid corrections to the fine level. Our study is concerned with this case. Because the final fine–grid correction is the sum of all the coarse–grid corrections (after being prolongated), we thus introduce errors which are essentially of the high–frequency type.

The present study is essentially based on the *dissipative properties* of the RK4 scheme of the *highest fine–grid frequency mode*. We thus present a simplified study that does not account for the entire spectrum of the fine–grid high–frequency modes. It appears, in fact, that in the hyperbolic context, the smoothing concept is less essential than in the elliptic context. Indeed, this can be related to the physical effects that are quite different in these two cases. Elliptic problems are related to pure relaxation phenomena. For hyperbolic equations, as the unsteady Euler equations, the convection phenomena play the major role, and the multigrid theory developed in the elliptic context is not directly applicable. This remark has also been done by other authors as E. Turkel [17] and A. Jameson [8], and it is confirmed by many numerical experiments; we also show this by a more complete study (given in appendix) considering all the fine–grid high–frequency modes.

1.2 The "Full Multigrid" algorithm

The previous basic algorithm can be used directly or can be generalized to define the "Full Multigrid" technique (or nested iterations). This permits to

more completely account for all the information we get at each grid–level. More precisely, one attempts to approach more closely the final solution from a better initialization at each level.

In this technique, the number of solution steps is the same as the number of grid levels. After each of these steps, we get a coarse–grid approximation of the final fine–grid solution. At each grid level k, starting from the coarsest one, one computes an approximate solution by applying the k–grid algorithm described previously, the interpolate of the approximate solution obtained by the previous step at level $k-1$ be the initial guess; for the first step, the initial guess corresponds to uniform flow discretized on the coarsest level. Thus, for this step, the algorithm used to compute the approximate solution is a 1–grid algorithm.

This technique allows to get a good approximate solution at each step, this cannot be obtained by the basic multigrid algorithm. Moreover, the convergence rate of this technique is independent of the number of nodes of the discretization, that means that the total computation work only linearly depends on the number of the fine–level unknowns.

2 1–D STABILITY ANALYSIS

2.1 The 1–D Conservation law model

2.1.1 Finite Volume approximation

Let us consider a 1–D conservation law

$$\begin{cases} \dfrac{\partial u}{dt}(x,t) + \dfrac{\partial}{\partial x} f(u)(x,t) = 0 \ , & \text{on } I\!R \times]0,+\infty[\ , \\ u(x,0) = u_0(x) \ , & \text{on } I\!R \ , \end{cases} \tag{7}$$

where $u = u(x,t)$, f is a function which can be non linear w.r.t. u; the second equation corresponds to the initial condition at time $t = 0$. This initial condition is supposed to be periodic w.r.t. x, with the period equal to 1, so as to restrict the study on the interval $]0,1[$, without additional boundary conditions.

The interval $]0,1[$ is regularly discretized with a space step $\Delta x = 1/N$, $N \in I\!N^*$ and we denote by $x_j = j\,\Delta x$, $j = 0,\ldots,N$ the discretization nodes.

Control volumes, or cells, are denoted by $\mathcal{C}_j$ and defined in the 1–D case as the intervals

$$\begin{aligned} \mathcal{C}_j &=]x_{j-\frac{1}{2}}, x_{j+\frac{1}{2}}[\ , \quad j = 1,\ldots,N-1 \ , \\ \mathcal{C}_0 &= [x_0, x_{\frac{1}{2}}[\ , \\ \mathcal{C}_N &=]x_{N-\frac{1}{2}}, x_N[\ , \end{aligned}$$

with $x_{j\pm\frac{1}{2}} = x_j \pm \Delta x/2$.

For a fixed value of time t, $t > 0$, and if we suppose $\partial u/\partial t$ to be a constant over each cell C_j, whose value is the node value at x_j, we obtain, after integration on each cell C_j, $j = 1, \ldots, N-1$

$$\Delta x \times \frac{\partial u}{dt}(x_j, t) + \left[f(u)(x^-_{j+\frac{1}{2}}, t) - f(u)(x^+_{j-\frac{1}{2}}, t) \right] = 0 \ , \tag{8}$$

We suppose here that $f(u)(\cdot, t)$ is non continuous at the nodes $x_{j\pm\frac{1}{2}}$ of the interface of the cell C_j, but we know the right limit value

$$f(u)(x^+_{j\pm\frac{1}{2}}) = \lim_{\substack{x \to x_{j\pm\frac{1}{2}} \\ x > x_{j\pm\frac{1}{2}}}} f(u)(x) \ ,$$

and the left limit value

$$f(u)(x^-_{j\pm\frac{1}{2}}) = \lim_{\substack{x \to x_{j\pm\frac{1}{2}} \\ x < x_{j\pm 1/2}}} f(u)(x) \ .$$

In addition, the following boundary and initial conditions are imposed

$$\begin{aligned} u(0,t) &= u(1,t) \ , \quad \text{(periodicity)} \\ u(x_j, 0) &= u_0(x_j) \ . \end{aligned}$$

On C_0, (8) can be written by

$$\frac{\Delta x}{2} \frac{\partial u}{\partial t}(0,t) + \left[f(u)(x^-_{\frac{1}{2}}, t) - f(u)(x^+_0, t) \right] = 0 \ ,$$

and on C_N, we have

$$\frac{\Delta x}{2} \frac{\partial u}{\partial t}(1,t) + \left[f(u)(x^-_N, t) - f(u)(x^+_{N-\frac{1}{2}}, t) \right] = 0 \ .$$

The time–continuous space–discretized system associated with (7) is expressed as follows

$$\frac{d}{dt} u_j(t) = -\frac{1}{\Delta x} R_j(u(t)) \ , \quad j = 1, \ldots, N-1 \ .$$

This is a system of ordinary differential equations in which $u_j(t) = u(x_j, t)$ and $R_j(u(t))$ is an approximation of $f(u)(x_{j+\frac{1}{2}}, t) - f(u)(x_{j-\frac{1}{2}}, t)$.

2.1.2 The time scheme

The 4–steps Runge–Kutta scheme employed here is a low–memory–storage linearized scheme, depending on fixed and constant parameters: it permits to

compute $u^{n+1} = (u_j{}^{n+1})_{j=1,\cdots,N} = (u(x_j, t_{n+1}))_{j=1,\cdots,N}$ at time t_{n+1}, starting from the initial iterate $u^n = (u_j{}^n)_{j=1,\cdots,N} = (u(x_j, t_n))_{j=1,\cdots,N}$ as the following

$$\begin{aligned} u^{(0)} &\stackrel{\text{def}}{=} u^n \ , \\ u^{(k)} &= u^{(0)} - \alpha_k \frac{\Delta t}{\Delta x} R(u^{(k-1)}) \ , \quad k = 1, \ldots, 4 \ , \\ u^{n+1} &\stackrel{\text{def}}{=} u^{(4)} \ , \end{aligned} \tag{9}$$

where

- $R(u^{(k-1)}) = \left(R_j(u^{(k-1)})\right)_j$ is the residual,
- $\Delta t = t_{n+1} - t_n$ is the time step which has a limited value due to stability conditions,
- α_k , $k = 1, \ldots, 4$, are the RK4 parameters, $0 < \alpha_k \leq 1$, $\alpha_4 = 1$.

We can show that for the classical parameters $\alpha_k = 1/(4 - k + 1)$, the RK4 method is fourth order accurate in time in the linear case (i.e. if f is a linear function of u). When we fix the parameter $\alpha_3 = 1/2$, it can be shown that the corresponding RK4 method is second–order accurate in time in both linear and non linear cases.

2.1.3 Spatial approximation schemes

For simplicity, we now only consider the linear case $f(u) = c\,u$ ($c > 0$). We thus have the well known advection equation $u_t + c\,u_x = 0$ that is the classical model for the analysis of both accuracy and stability of hyperbolic problems.

The scheme is fully determined as soon as we have the approximate values of

$$f(u^-_{j+\frac{1}{2}}) - f(u^+_{j-\frac{1}{2}}) \ ,$$

or equivalently

$$u^-_{j+\frac{1}{2}} - u^+_{j-\frac{1}{2}} = u(x^-_{j+\frac{1}{2}}, t) - u(x^+_{j-\frac{1}{2}}, t) \ .$$

Centered spatial scheme

$$\text{(C)} \qquad \left\{ \begin{array}{rcl} u^-_{j+\frac{1}{2}} &=& \dfrac{u_j + u_{j+1}}{2} \ , \\ u^+_{j-\frac{1}{2}} &=& \dfrac{u_j + u_{j-1}}{2} \ . \end{array} \right. \tag{10}$$

Here we can see that we suppose u to be continuous at each interface nodes of the cells. It can also be observed that this approximation does not take into account the direction of the wave propagation (i.e. the sign of the wave speed c).

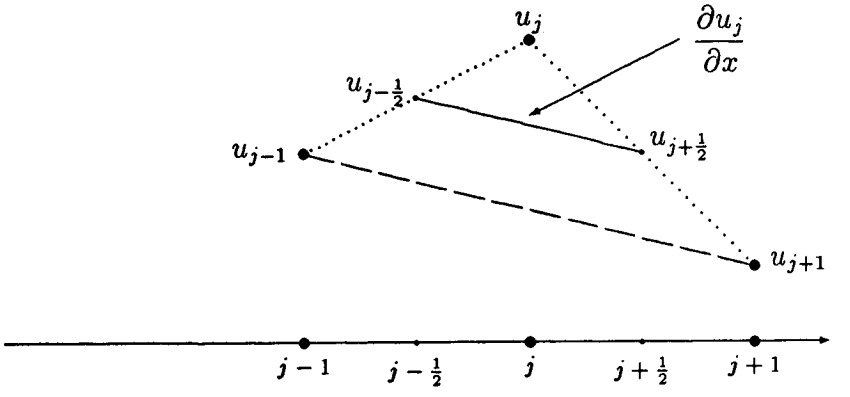

Figure 1: Centered scheme (C)

By a local Taylor's series expansion at x_j, we get

$$\frac{u_{j+1} - u_{j-1}}{2\Delta x} = u_x + \frac{\Delta x^2}{6} u_{xxx} + o(\Delta x^2) ,$$

showing that the formula is second order accurate. The slope u_x evaluated in this way is represented on figure 1.

First-order accurate upwind scheme

$$(\mathbf{D_1}) \qquad \begin{cases} u^-_{j+\frac{1}{2}} &= u_j , \\ u^+_{j-\frac{1}{2}} &= u_{j-1} . \end{cases} \tag{11}$$

Here, the direction of the wave propagation is respected; the values assigned to u at the node x only depends on the values at preceding nodes. This supposes that u is considered to be constant on each cell.

The local Taylor's series expansion at the node x_j related to this approximation is

$$\frac{u_j - u_{j-1}}{\Delta x} = u_x - \frac{\Delta x}{2} u_{xx} + o(\Delta x) ,$$

thus, the corresponding scheme is only first-order accurate. The slope u_x evaluated in this way is represented on figure 2.

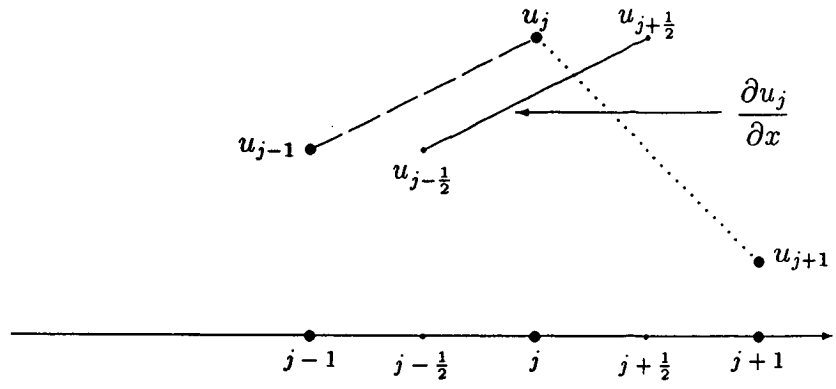

Figure 2: First order accurate upwind scheme $(\mathbf{D_1})$

Second order accurate half upwind scheme

$$(\mathbf{D_2}) \qquad \begin{cases} u^-_{j+\frac{1}{2}} &= u_j + \dfrac{\Delta x}{2}\left(\dfrac{u_{j+1}-u_{j-1}}{2\Delta x}\right), \\ u^+_{j-\frac{1}{2}} &= u_{j-1} + \dfrac{\Delta x}{2}\left(\dfrac{u_j-u_{j-2}}{2\Delta x}\right). \end{cases} \tag{12}$$

If we compare these values to those given by the scheme $(\mathbf{D_1})$, we can see that they are no more constant on each cell. We define here some local centered slopes at the node x_j (respectively to the approximate value $u^-_{j+1/2}$), and at the node x_{j-1} (respectively to $u^+_{j-1/2}$). They are obtained by assuming u to vary linearly on each interval $]x_j, x_{j+1}[$ (P_1 Galerkin approximation). The derivatives of u w.r.t. x are thus considered to be piecewise constant on each interval $]x_j, x_{j+1}[$ and the prescribed value is $(u_{j+1}-u_j)/\Delta x$. The local slopes at each node x_j are deduced by averaging the right and left Galerkin slopes associated with this node. So, the local slope at the node x_j is taken to be

$$\frac{1}{2}\left(\frac{u_j-u_{j-1}}{\Delta x}+\frac{u_{j+1}-u_j}{\Delta x}\right)=\frac{u_{j+1}-u_{j-1}}{2\Delta x}\,.$$

The local Taylor's series expansion at the node x_j related to this scheme is

$$\frac{1}{4\Delta x}\left(u_{j+1}+3u_j-5u_{j-1}+u_{j-2}\right)=u_x-\frac{\Delta x^2}{12}\,u_{xxx}+o(\Delta x^2)\,.$$

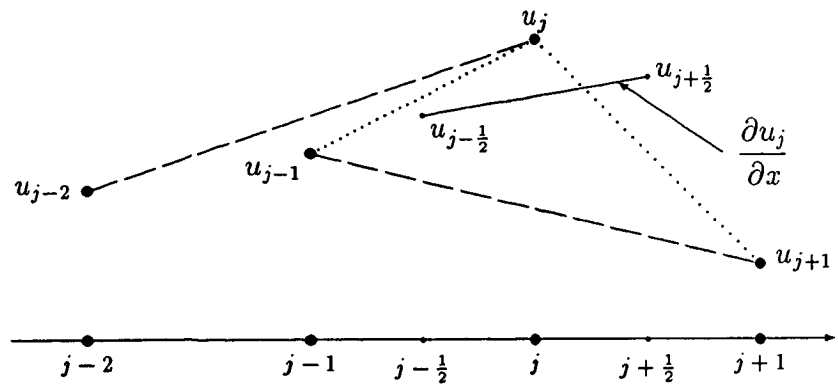

Figure 3: Second order half upwind scheme $(\mathbf{D_2})$

The formula is therefore second–order accurate. The slope u_x approximated in this way is represented on figure 3.

$(\mathbf{D_1})$ and $(\mathbf{D_2})$ can be rewritten in function of the centered scheme (C). This gives for scheme $(\mathbf{D_1})$

$$\frac{u_j - u_{j-1}}{\Delta x} = \left(\frac{u_{j+1} - u_{j-1}}{2\Delta x}\right) + \frac{\Delta x}{2}\left(\frac{-u_{j-1} + 2u_j - u_{j+1}}{\Delta x^2}\right) . \qquad (13)$$

The second term appearing in the right hand side is an approximation of $(\Delta x/2)\,\partial^2 u/\partial x^2$ at the node (x_j, t). This explains why the scheme is very dissipative. For scheme $(\mathbf{D_2})$ we have

$$\frac{u_{j+1} + 3u_j - 5u_{j-1} + u_{j-2}}{4\Delta x} = \frac{1}{2}\left(\frac{u_{j+1} - u_{j-1}}{2\Delta x}\right) + \frac{1}{2}\left(\frac{u_{j-2} - 4u_{j-1} + 3u_j}{2\Delta x}\right) . \qquad (14)$$

$(\mathbf{D_2})$ is a second–order accurate half–upwind scheme usually referred to as the Fromm scheme whose the general expression is

$$(1-\beta)\left(\frac{u_{j+1} - u_{j-1}}{2\Delta x}\right) + \beta\left(\frac{+u_{j-2} - 4u_{j-1} + 3u_j}{2\Delta x}\right) , \qquad (15)$$

with $\beta \in [0, 1]$.

For $\beta = 1/2$, we have $(\mathbf{D_2})$, $\beta = 0$ corresponds to (C), and the second–order accurate full upwind scheme is obtained when $\beta = 1$; in the latter case,

the approximate values of u at the interfaces of the cell are

$$\left\{ \begin{array}{rcl} u^-_{j+\frac{1}{2}} & = & u_j + \dfrac{\Delta x}{2}\left(\dfrac{u_j - u_{j-1}}{\Delta x}\right) , \\ u^+_{j-\frac{1}{2}} & = & u_{j-1} + \dfrac{\Delta x}{2}\left(\dfrac{u_{j-1} - u_{j-2}}{\Delta x}\right) . \end{array} \right. \tag{16}$$

By "full upwind" scheme, we mean that the slopes also are approximated by upwind differences: they are also deduced from the Galerkin approximation but the local slope at the node x_i is taken to be equal to the left slope defined at the node x_i.

When $\beta = 1/3$, we obtain a third–order accurate scheme that has been studied by J-A. Désidéri et al. in [5].

Remark 2.1 *When the approximations* (C) *and* $(\mathbf{D_2})$ *are used and combined with the Euler explicit method, the resulting schemes are* unconditionally unstable. *Using* $(\mathbf{D_1})$ *the scheme is stable under the CFL condition. We shall see that when using the RK4 method for time integration, the resulting scheme associated with the spatial approximations* (C) *and* $(\mathbf{D_2})$ *become stable, because of the introduction of more dissipative terms.*

2.1.4 Local Fourier mode analysis

In the different steps of the RK4 method defined in (9), we have the quantity $(\Delta t\,/\,\Delta x)\,R(u)$ to be evaluated for many values of u. Considering a unique Fourier mode, $\hat{u} = e^{ip\Delta x}$, we have (diagonalization)

$$\frac{\Delta t}{\Delta x} R(\hat{u}) = -z\,\hat{u} , \tag{17}$$

where z is a complex number depending on the frequency $\theta = p\Delta x$, it corresponds to the associated opposite eigenvalue of $R(\hat{u})\,/\,\Delta x$ multiplied by Δt. More precisely, the values of z are

For the scheme $(\mathbf{D_1})$ $\quad z = z_1 = -\sigma(1 - e^{-i\theta}) = 2\,i\,\sigma\,e^{i\frac{\theta}{2}}\sin\frac{\theta}{2}$,

For the scheme $(\mathbf{D_2})$ $\quad z = z_2 = -2\,\sigma\sin^4\frac{\theta}{2} - i\,\sigma\,\sin\theta\,(1 + \sin^2\frac{\theta}{2})$.

where $\sigma = c\,\Delta t/\Delta x$ is the Courant number.

In the general case, one RK4 iteration yields to the following equality

$$\hat{u}^{n+1} = g(z)\,\hat{u}^n ,$$

where $g(z)$ denotes the amplification factor which can be rewritten as

$$g(z) = 1 + z + \alpha_3\,z^2 + \alpha_3\,\alpha_2\,z^3 + \alpha_3\,\alpha_2\,\alpha_1\,z^4 . \tag{18}$$

The stability domain of the RK4 method is the following set

$$\mathcal{D} = \{z \in \mathcal{C};\ |g(z)| < 1\}\ , \tag{19}$$

where $\mathcal{C}$ denotes the complex plane.

If an approximation is chosen, we can determine the locus of z for the different values of θ; we can thus evaluate the maximum allowable value of the Courant number, that is

$$\sigma_{max} = \left(c\frac{\Delta t}{\Delta x}\right)_{max}$$

for which $z \in \mathcal{D}$, $\forall\theta$.

2.2 Optimization of the RK4 scheme

This optimization is not the same if we use a one–grid or a multigrid technique.

2.2.1 1–grid case

Because of the conditional stability of the explicit pseudo–unsteady methods, we need many time steps to get a good approximate solution, i.e. the convergence rate is often very slow and depends on the grid size. This means that the stiffness of such methods lies in the restricted (small) values of allowable time steps.

One way to diminish this time–step limitation, is to use Runge–Kutta methods that allow larger stability domains if the parameters are judiciously chosen. Moreover, and this is essential in our analysis, Runge–Kutta methods have good dissipative properties near the maximum value of the Courant number. The way we choose the different parameters depends on the approximation we use.

It is known that the spectral set of centered discrete operators lies on the imaginary axis of the complex plan; in this case, the standard RK4 scheme ($\alpha_k = 1/(4-k+1)$) is well adapted, because the stability domain has its greater size on the imaginary axis. However, concerning the discrete operators of *upwind* type, the eigenvalues have a *non zero real part* and then, the standard RK4 scheme is no longer the most advantageous. Thus we have to determine other values for the α_k, so as to get a larger size of the stability domain on the real axis too. These values depend on both the size and shape of the spectral set of the discrete upwind operator.

In the figures 4 and 5, we can see the stability domains associated respectively to the approximations $(\mathbf{D_1})$ and $(\mathbf{D_2})$ with respective maximum Courant number (CFL) $\sigma^1_{max} = 2.2105$ and $\sigma^2_{max} = 1.9186$ for the following RK4 parameters

$$\alpha_1 = 0.11,\ \alpha_2 = 0.2766\ldots,\ \alpha_3 = 0.5,\ \alpha_4 = 1\ .$$

(superscripts refer to the degree of accuracy of the upwind approximations).

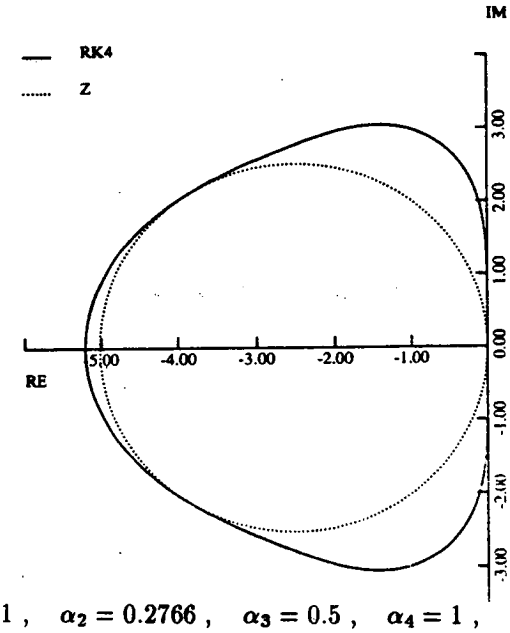

$\alpha_1 = 0.11$, $\alpha_2 = 0.2766$, $\alpha_3 = 0.5$, $\alpha_4 = 1$, $\sigma^1_{max} = 2.5105$.

Figure 4: RK4 stability domain with $(\mathbf{D_1})$ as spatial approximation.

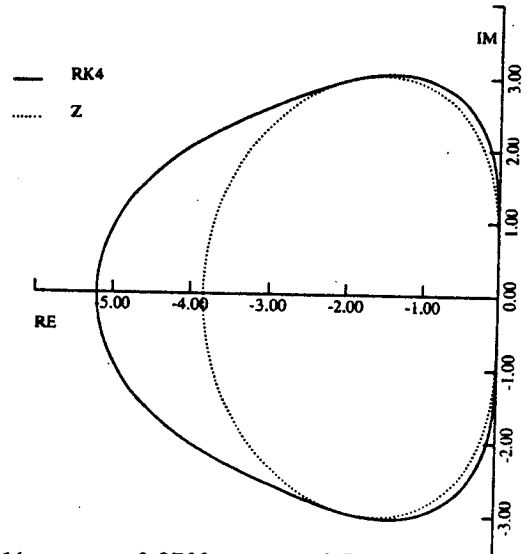

$\alpha_1 = 0.11$, $\alpha_2 = 0.2766$, $\alpha_3 = 0.5$, $\alpha_4 = 1$, $\sigma^e_{max} = 1.9186$.

Figure 5: RK4 stability domain with $(\mathbf{D_2})$ as spatial approximation.

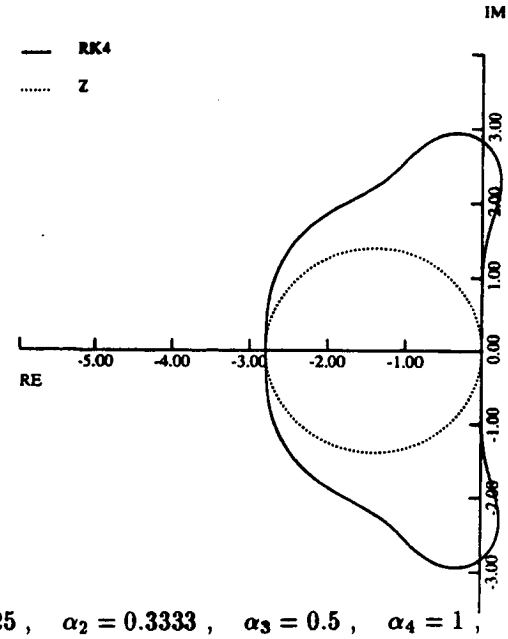

$\alpha_1 = 0.25$, $\alpha_2 = 0.3333$, $\alpha_3 = 0.5$, $\alpha_4 = 1$, $\sigma^2_{max} = 1.39264$.

Figure 6: RK4 stability domain with $(\mathbf{D_1})$ as spatial approximation.

The first two coefficients α_1, α_2 where obtained by trial–and–error around the standard values 1/4 and 1/3. Notice that the stability domains are well adapted to the shape of both first (figure 4), and second (figure 5) order accurate upwind spectral sets.

For the standard RK4 method ($\alpha_k = 1/(4-k+1)$,) which is optimal for the centered scheme (C), we find when using $(\mathbf{D_1})$ and $(\mathbf{D_2})$ the following maximum CFL (see figures 6 and 7)

$$\sigma^1_{max} = 1.39264 \ , \quad \sigma^2_{max} = 1.38465 \ .$$

We can notice that these values are about 30% less than the previous ones. Although the standard RK4 scheme (which is fourth order accurate in time in the linear case) is well adapted to centered approximations, the best RK4 scheme for upwind spatial approximations and allowing large time steps is only second order accurate in time.

In conclusion, the optimization of the RK4 scheme is driven by the following criterion

$[\mathbf{C_1}]$ *Given a spatial approximation, find the coefficients α_k such as the stability domain is as large as possible, i.e. so as to maximize the value of the Courant number σ_{max}.*

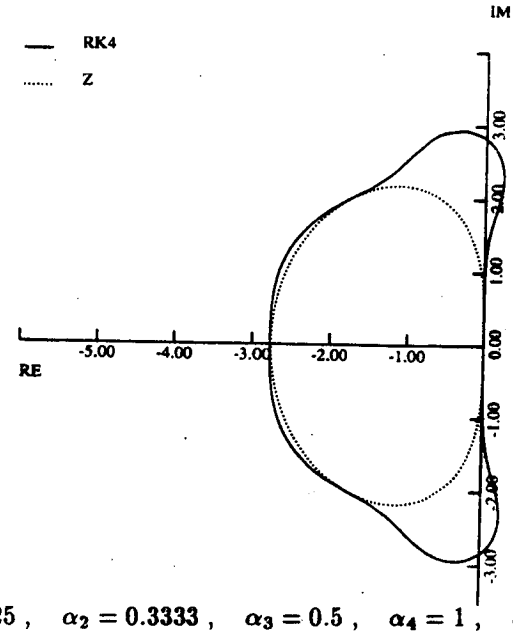

$\alpha_1 = 0.25$, $\alpha_2 = 0.3333$, $\alpha_3 = 0.5$, $\alpha_4 = 1$, $\sigma^2_{max} = 1.38465$.

Figure 7: RK4 stability domain with $(\mathbf{D_2})$ as spatial approximation.

This criterion can be expressed by maximizing the following function

$$z \in \mathcal{D} \longrightarrow |g(z)| ,$$

with $z = z_1$ for the scheme $(\mathbf{D_1})$, and $z = z_2$ for the scheme $(\mathbf{D_2})$. These coefficients are

$$\alpha_1 = 0.10,\ \alpha_2 = 0.26,\ \alpha_3 = 0.5,\ \alpha_4 = 1,\ \text{and}\ \sigma^1_{max} = 2.6756 ,$$

for the spatial approximation $(\mathbf{D_1})$, and

$$\alpha_1 = 0.12,\ \alpha_2 = 0.26,\ \alpha_3 = 0.5,\ \alpha_4 = 1,\ \text{and}\ \sigma^2_{max} = 2.0763 .$$

for the approximation $(\mathbf{D_2})$.

The corresponding stability domains are shown in figures 8 and 9.

A criterion for multigrid purposes

In the multigrid context [10, 16], the optimization criteria are more severe. We still want $[\mathbf{C_1}]$ to be satisfied, but we require in addition that the RK4 scheme have good smoothing properties especially at the highest frequency.

Thus, for fixed, and sufficiently large CFL number σ, we want the following criterion to be realized

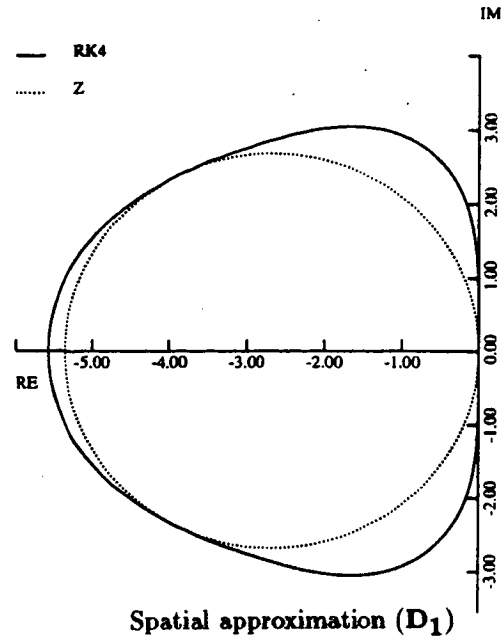

Spatial approximation ($\mathbf{D_1}$)

$\alpha_1 = 0.10$, $\alpha_2 = 0.26$, $\alpha_3 = 0.5$, $\alpha_4 = 1.0$, $\sigma^1_{max} = 2.6756$

Figure 8: RK4 stability domain related to the criterion $[\mathbf{C_1}]$.

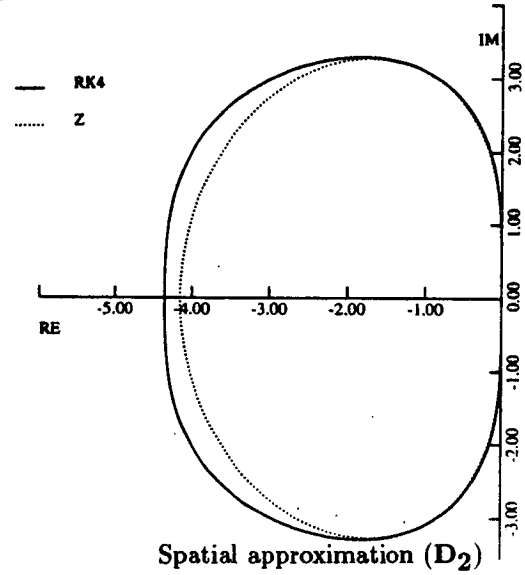

Spatial approximation ($\mathbf{D_2}$)

$\alpha_1 = 0.12$, $\alpha_2 = 0.26$, $\alpha_3 = 0.5$, $\alpha_4 = 1.0$, $\sigma^2_{max} = 2.0763$

Figure 9: RK4 stability domain related to the criterion $[\mathbf{C_1}]$.

[C_2] *Given a spatial approximation scheme, find the optimal RK4 coefficients α_k, such as the resulting full scheme is stable and has good smoothing properties.*

Optimization of the coefficients

It is based on the following idea: because we want a good damping of the highest frequency modes, we can find the best coefficients by studying the behavior of the amplification factor in the neighborhood of the highest frequency i.e. for $\theta = \pi$.

We refer to the study by Jameson [10], in the linear and scalar context for the amplification factor related to one multigrid cycle. This simplified study is also validated a posteriori by some numerical experiments comparing results obtained with the present analysis and those obtained by an analysis done for all high–frequency modes. In both studies, the RK4 coefficients have very close values but the optimal CFL number is quite different since it corresponds in the full analysis to nearly half the value of the Courant number obtained with our method. As a direct consequence the convergence rate is also reduced by a factor of 1/2. We can thus say that the criterion [C_2] is sufficient for the optimization of the different parameters. The 3–D extension [2] of the method presented in [12] (chapter 1), confirms already the convergence and efficiency gains that were observed in 2–D.

From now on, we are only concerned with consistent ($\alpha_4 = 1$), and second–order accurate ($\alpha_3 = 1/2$) RK4 schemes.

Once we have our spatial approximation scheme, we can notice that

$$|g(z)| = G(\sigma, \theta, \alpha_1, \alpha_2) \ , \quad \text{with} \ \begin{cases} 0 \leq \theta \leq 2\pi \ , \\ \sigma > 0 \ , \\ \alpha_1, \ \alpha_2 \ \in]0, 1[\ . \end{cases} \tag{20}$$

As G is an odd and periodic function w.r.t. θ, we can restrict our study to $\theta \in [0, \pi]$.

Given σ, α_1, α_2, the function

$$\theta \in [0, \pi] \rightarrow G(\sigma, \theta, \alpha_1, \alpha_2) \ , \tag{21}$$

allows us to determine the smoothing properties of the RK4 scheme. These properties depend also on the value of σ; its maximal value does not indeed yield evidently to the optimality of the smoothing properties. Then, because the highest frequency mode corresponds to $\theta = \pi$, we have restricted our analysis to this value.

We are thus only interested in the study of the function

$$G_\pi \ : \ \sigma \rightarrow G_\pi(\sigma) = G(\sigma, \pi, \alpha_1, \alpha_2) \ , \tag{22}$$

with $\sigma \in [0, \sigma_{max}]$. If this function vanishes or has very small values for one (or many) value(s) of σ, that are denoted by $\tilde{\sigma}$, the optimization is then realized when

- $\sigma = \tilde{\sigma}$,
- and the given α_k we have fixed at the beginning.

If not, the function admits a too large strictly positive lower bound, the coefficients α_k must be discarded.

We can summerize the optimization of the parameters α_k and σ as the following rule

(i) Give a sufficiently large value of the CFL $\overline{\sigma}$,

(ii) Find the coefficients α_k such as for this fixed value $\overline{\sigma}$, the resulting RK4 scheme is stable (then we have $\sigma_{max} \geq \overline{\sigma}$).

(iii) Study of the function G_π. We can then meet the two following alternatives

- either this function has one or more "zeroes", and the coefficients found in (ii) have to be kept; then the optimal value of σ is chosen to be one of these zeroes,
- or this function has no zero, and the search is continued in step (ii), or (i).

Notice that the different steps of this optimization method are very close to each other. This means that we cannot do the steps separately. Realizing the criterion $[\mathbf{C_2}]$ is then not immediate.

We can see (figure 10) that the optimized coefficients α_k found in the one grid case (criterion $[\mathbf{C_1}]$) are not satisfying in the multigrid context. Indeed, for the RK4 scheme related to the $(\mathbf{D_2})$ approximation, the function G_π has strictly positive values and the corresponding curve of the amplification factor (figure 11) show that it has bad smoothing properties.

However, (see figures 12 and 13), the coefficients α_k found for the one grid RK4 scheme related to the spatial approximation $(\mathbf{D_1})$ are also available here because the function G_π has two zeroes $\tilde{\sigma}_1^1 = 1.7736$, $\tilde{\sigma}_2^1 = 1.9398$. We choose as the best value $\sigma = \tilde{\sigma}_1^1$ (the superscript refers to the order of accuracy of the spatial approximation).

For the RK4 scheme related to the spatial approximation $(\mathbf{D_2})$ one possible choice of the parameters is (see figures 14 and 15)

$$\alpha_1 = 0.10 \ , \quad \alpha_2 = 0.26 \ , \quad \alpha_3 = 0.5 \ , \quad \alpha_4 = 1.0 \ ,$$

with $\sigma = \tilde{\sigma}^2 = \tilde{\sigma}_1^1 = 1.7736$ and $\sigma_{max}^2 = 1.9329$.

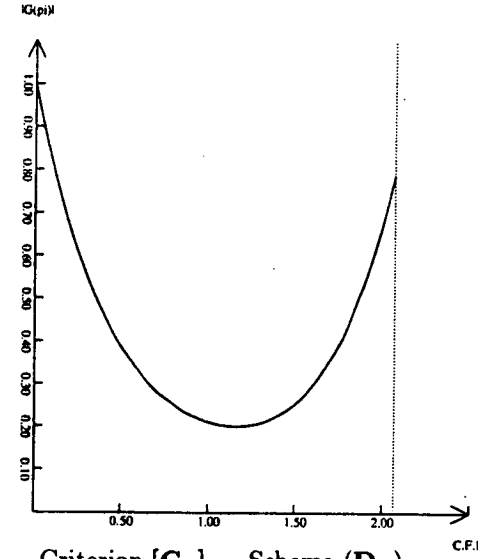

Criterion $[\mathbf{C_2}]$ — Scheme $(\mathbf{D_2})$

$\sigma^2_{max} = 2.0763$

$\alpha_1 = 0.12\,, \quad \alpha_2 = 0.26\,, \quad \alpha_3 = 0.5\,, \quad \alpha_4 = 1.0$

Figure 10: Curve of the function $G_\pi \;:\; \sigma \in [0, \sigma_{max}] \longrightarrow G(\sigma, \pi, \alpha_1, \alpha_2)$.

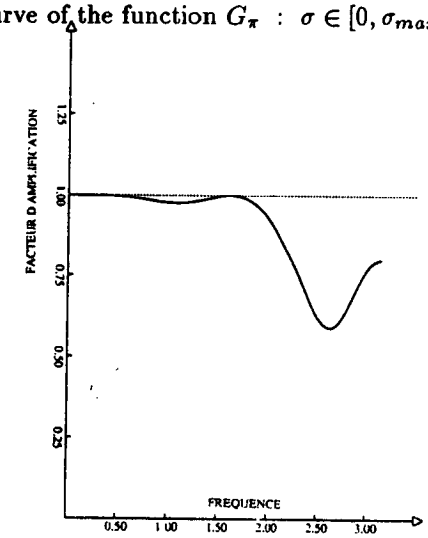

Criterion $[\mathbf{C_2}]$ — Scheme $(\mathbf{D_2})$

$\sigma^* = \sigma^2_{max}$

$\alpha_1 = 0.12\,, \quad \alpha_2 = 0.26\,, \quad \alpha_3 = 0.5\,, \quad \alpha_4 = 1.0$

Figure 11: Curve of the amplification factor $\theta \in [0, \pi] \longrightarrow G(\sigma^*, \theta, \alpha_1, \alpha_2)$

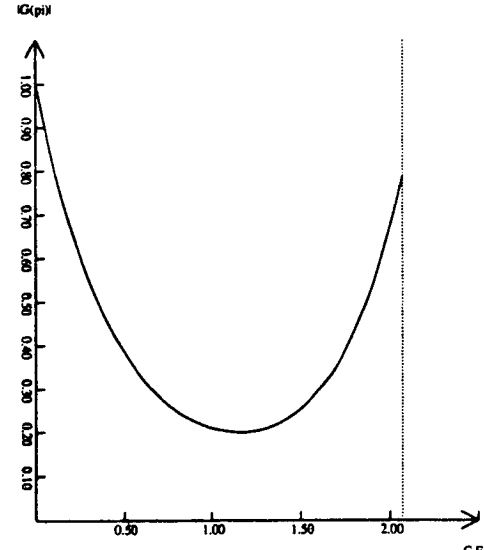

Criterion $[\mathbf{C_2}]$ — Scheme $(\mathbf{D_1})$

$\sigma^1_{max} = 2.6756$, $\widetilde{\sigma}^1_1 = 1.7736$, $\widetilde{\sigma}^1_2 = 1.9398$

$\alpha_1 = 0.10$, $\alpha_2 = 0.26$, $\alpha_3 = 0.5$, $\alpha_4 = 1.0$

Figure 12: Curve of the function G_π : $\sigma \in [0, \sigma_{max}] \longrightarrow G(\sigma, \pi, \alpha_1, \alpha_2)$.

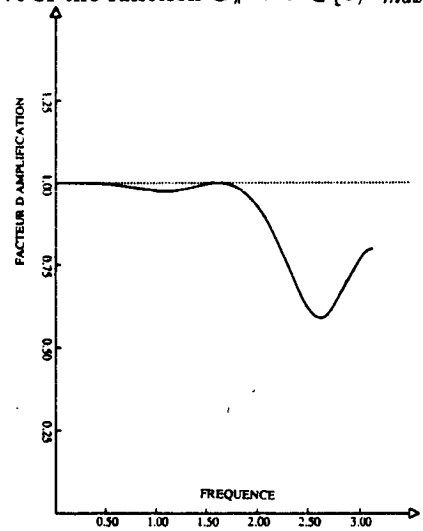

Criterion $[\mathbf{C_2}]$ — Scheme $(\mathbf{D_1})$

$\alpha_1 = 0.10$, $\alpha_2 = 0.26$, $\alpha_3 = 0.5$, $\alpha_4 = 1.0$, $\sigma^* = \widetilde{\sigma}^1_1$

Figure 13: Curve of the amplification factor $\theta \in [0, \pi] \longrightarrow G(\sigma^*, \theta, \alpha_1, \alpha_2)$

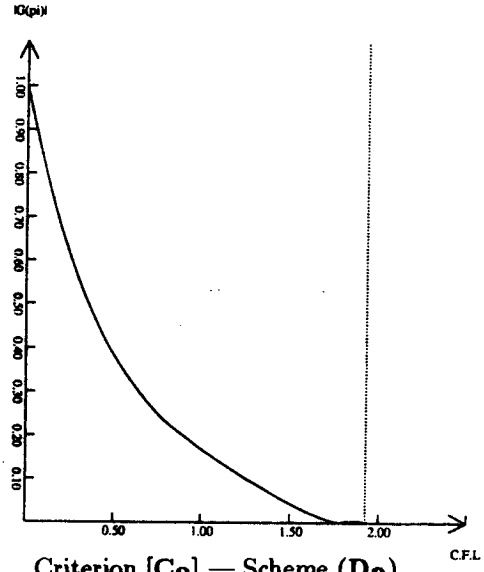

Criterion $[\mathbf{C_2}]$ — Scheme $(\mathbf{D_2})$

$\sigma^2_{max} = 1.9329$, $\widetilde{\sigma}^2 = 1.7736$

$\alpha_1 = 0.10$, $\alpha_2 = 0.26$, $\alpha_3 = 0.5$, $\alpha_4 = 1.0$

Figure 14: Curve of the function G_π : $\sigma \in [0, \sigma_{max}] \longrightarrow G(\sigma, \pi, \alpha_1, \alpha_2)$.

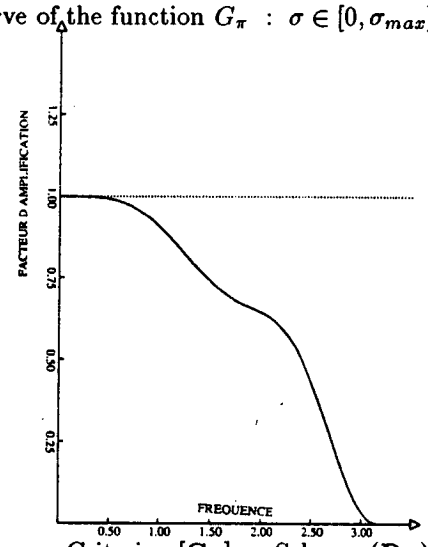

Criterion $[\mathbf{C_2}]$ — Scheme $(\mathbf{D_2})$

$\sigma^* = \widetilde{\sigma}^2$

$\alpha_1 = 0.10$, $\alpha_2 = 0.26$, $\alpha_3 = 0.5$, $\alpha_4 = 1.0$

Figure 15: Curve of the amplification factor $\theta \in [0, \pi] \longrightarrow G(\sigma^*, \theta, \alpha_1, \alpha_2)$

3 2–D EXTENSION

The objective to be reached here is to try to define a few principles for simply extending the results obtained in the previous 1–D study to the solution of the 2–D Euler equations when using unstructured triangular P1 Finite Element discretizations. We recall that by unstructured mesh we mean that a given node of the mesh may be the vertex of a non constant number of triangles (in 2–D) or tetrahedra (in 3–D).

As in the 1–D context, a RK4 method is used for the time integration. The spatial approximation scheme is of upwind type and will be briefly presented. For more details concerning the spatial approximations and the resulting basic scheme, we refer to [6] and [12] (chapter 1).

3.1 First order accurate upwind scheme

The unsteady 2–D Euler equations are written in conservative form

$$\frac{\partial}{\partial t}W + \frac{\partial}{\partial x}(F(W)) + \frac{\partial}{\partial y}(G(W)) = 0 \ , \tag{23}$$

with

$$\begin{aligned} W &= (\rho, \rho u, \rho v, E)^t \ , \\ F(W) &= (\rho u, \rho u^2 + p, \rho u v, u(E+p))^t \ , \\ G(W) &= (\rho v, \rho u v, \rho v^2 + p, \rho u v, v(E+p))^t \ , \end{aligned}$$

where p is the pressure, ρ the density, E the total energy, and (u, v) the components of the material speed $\overrightarrow{V}$ of the flow. In addition, the state equation for a perfect gas is employed

$$p = (\gamma - 1)\left(E - \frac{1}{2}\rho(u^2 + v^2)\right) \ , \tag{24}$$

with a specific heat ratio $\gamma = 1.4$ for air.

Let Ω be the computational domain that is discretized by triangular Finite Elements, where the nodes A_i are located at the vertices of the triangles. Let us denote $W(A_i, t) = W_i(t)$.

For each node A_i, we define a cell C_i as the area limited by the medians of each triangle having A_i as a vertex (see figure 16). Let us fix t, and assume $\partial W/\partial t$ to be constant on each cell C_i, then we obtain, integrating the equations (23) on C_i

$$\frac{\partial W}{\partial t}(A_i) = -\frac{1}{\text{area}(C_i)} \sum_{j=1}^{N_i} \Phi(W_i, W_j, \overrightarrow{\eta}^{ij}) \ , \tag{25}$$

where

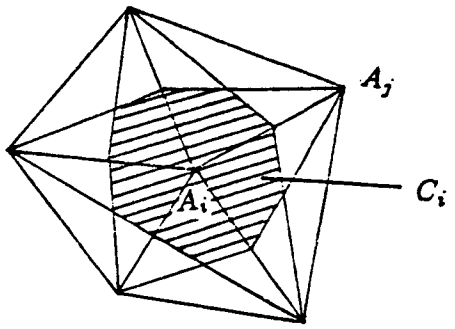

Figure 16: Cell C_i

- N_i is the number of neighboring nodes of A_i,
- $\overrightarrow{\eta}^{ij} = (\eta_x^{ij}, \eta_y^{ij})$ with $\eta_x^{ij} = \int_{\partial C_i \cap \partial C_j} \nu_x \, d\sigma$, $\eta_y^{ij} = \int_{\partial C_i \cap \partial C_j} \nu_y \, d\sigma$,
- $\overrightarrow{\nu} = (\nu_x, \nu_y)$ the outward unit normal vector of C_i,
- Φ is a numerical flux function which is consistent to $F\,\eta_x + G\,\eta_y$.

We use the following flux splitting [18]

$$\Phi(U, V, \overrightarrow{\eta}) = \frac{1}{2}\,\eta_x\,[F(U)+F(V)]+\frac{1}{2}\,\eta_y\,[G(U)+G(V)]+\frac{1}{2}\left|P(\frac{U+V}{2})\right|(U-V)\,, \tag{26}$$

(see [12] (chapter 1) for more details).

We recall that the first order accurate upwind spatial approximation denoted by $(\mathcal{D}_1)$ is obtained when we set

$$\begin{aligned} U &= W_i\,, \\ V &= W_j\,. \end{aligned} \tag{27}$$

3.2 Second–order upwind scheme

The second order accurate version is obtained via the MUSCL approach [7] due to B. van Leer and that has been adapted to the Finite Element context by L. Fezoui [6].

For this purpose, we compute an approximated gradient of W, $\overrightarrow{\nabla} W = (\overline{W}_x, \overline{W}_y)$, for each vertex A_i using a Galerkin linear interpolation of W over

each triangle having A_i as a vertex

$$\overrightarrow{\nabla} W(A_i) = (\overline{W}_x(A_i), \overline{W}_y(A_i)) ,$$

with

$$\overline{W}_x(A_i) = \frac{\int_{supp(i)} \frac{\partial W}{\partial x}\, dx\, dy}{\int_{supp(i)} dx\, dy} , \quad \overline{W}_y(A_i) = \frac{\int_{supp(i)} \frac{\partial W}{\partial y}\, dx\, dy}{\int_{supp(i)} dx\, dy} .$$

$supp(i)$ represents the union of all the triangles having A_i as a vertex.

At each segment (A_i, A_j), we compute the following W's extrapolated values

$$\begin{aligned} W_{ij} &= W_i + \frac{1}{2} \overrightarrow{\nabla} W(A_i) . \overrightarrow{A_i A_j} , \\ W_{ji} &= W_j + \frac{1}{2} \overrightarrow{\nabla} W(A_j) . \overrightarrow{A_j A_i} . \end{aligned}$$

We can replace these values by limited ones $(\overline{W}_{ij}, \overline{W}_{ji})$ so as to avoid the too large variations of these gradients near the shocks (discontinuities). The resulting scheme is then only first order accurate near the shocks and second order accurate where the approximate solution is smooth. We refer to [11] (chapter 1) for more details concerning the limitation procedure.

The second order accurate upwind scheme, denoted by $(\mathcal{D}_2)$ is then obtained by setting

$$\left\{ \begin{array}{lcl} U &=& W_{ij} \quad (\text{or } \overline{W}_{ij}) , \\ V &=& W_{ji} \quad (\text{or } \overline{W}_{ji}) . \end{array} \right. \tag{28}$$

3.3 Stability condition

So as to accelerate the convergence rate up to the steady state, we also use local time steps [4]; a local time step is defined by applying a local stability condition, at each node A_i of the triangulation as in the following

$$\mathcal{V}_i \Delta t_i \leq \sigma^* h_i , \tag{29}$$

with

- $\mathcal{V}_i = \max_{k, A_k neighb. A_i} (\lambda_i, \lambda_k)$ the maximal wave speed at the node A_i, where

  $\lambda_j = \sqrt{u_j^2 + v_j^2} + c_j$ is the local wave speed at the node A_j,

  u_j and v_j are respectively the x and y components of the flow speed at the node A_j,

c_j holds for the local sound speed at the node A_j ,

- Δt_i is the local time step at the node A_i,
- σ^* is the value of the 1–D CFL number that depends on the RK4 scheme we use, $\sigma^* \leq \sigma_{max}$
- h_i is the lowest height from A_i of all the triangles having A_i as a vertex.

Notice that in 2–D and because $\mathcal{V}_i$ is no more constant, we cannot control the value of the real CFL number. This means that in the optimization rule described below, we will not take into account that we also have slower wave speeds.

3.4 2–D extension

For one grid methods, this extension is straightforward, we take for σ^* the CFL value we find in the 1–D analysis, i.e. the maximal value of the CFL related to the α_k parameters that yield a large stability domain.

In the multigrid context, we also extend the results obtained in the 1–D analysis by noticing that the computation of the numerical fluxes is in some sense a 1–D computation.

This extension is essentially based on the geometry of the mesh that can be characterized by introducing a new parameter $e \in [0, 1]$ depending on the structure of each element and defined as below:

Let T be any element of a given triangulation, S_1, S_2, S_3 be the three vertices of T.

We change the reference frame with, as a new origin, one of the three vertices S_i such as the side of the triangle S_iS_j is the largest one. The two new axis are then determined to be S_iS_j, (for the first new component x' and directed to S_j) and the height drawn from S_k, (for the second new component y' and directed to S_k) (see figure 17).

Let h_i, h_j and h_k denote the three heights of the triangle respectively drawn from S_i, S_j and S_k. The new coordinates of S_i, S_j and S_k are

$$S_i = (0,0),\ S_j = (1,0) \text{ and } S_k = (x_k, h_k)\ .$$

We define

$$e_T \stackrel{\text{def}}{=} \min(h_i, h_j, h_k) \quad \text{and} \quad e \stackrel{\text{def}}{=} \min_T(e_T)\ ,$$

where the minimum is taken over all the elements T of the triangulation.

Regular mesh

For a structured regular mesh, the value of e_T is uniform over all the triangulation, and $e = e_T$ for all T. We give (figures 18 to 20) some examples of typical values taken by e.

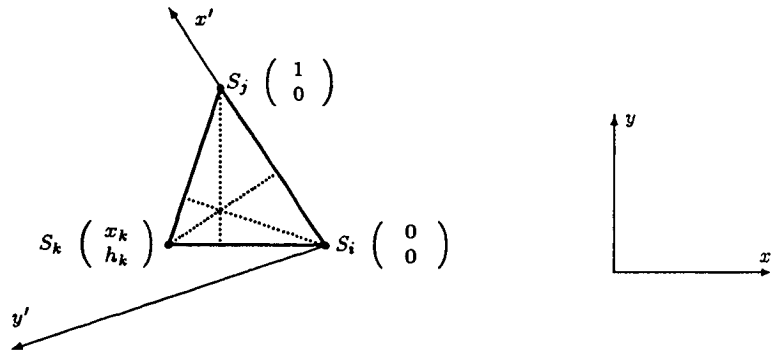

Figure 17: The new coordinate system.

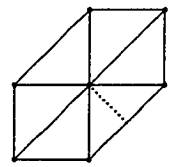

Figure 18: $\Delta x = \Delta y$, rectangular triangle, $e = \sqrt{2}/2$.

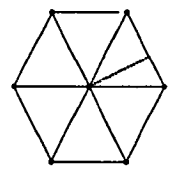

Figure 19: $\Delta x = \Delta y$, isoceles triangle, $e = 2\sqrt{5}/5$.

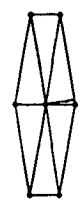

Figure 20: $\Delta x << \Delta y$, $e \simeq 1$.

Arbitrary mesh

For an arbitrary triangulation, it is impossible to know a priori the value of e. In this case, and to avoid the computation of e, we give an estimation of its most probable value. Thus an estimated value is fixed to be $\sqrt{2}/2$ and corresponds to the smallest currently met value in a triangulation.

Determination of the parameters

We shall describe here how to deduce the values of the different parameters σ^* and α_k from the 1–D analysis, when we set $e = \sqrt{2}/2$.

If σ denotes the fixed given CFL number, the local CFL number (in the x and y direction) takes its values a priori in $[0, \sigma]$; but globally, the most current values are taken in $[e\sigma, \sigma]$.

Knowing this variation, it is sufficient to modify the step 3) in the previous method for the criterion $[\mathbf{C_2}]$, by adding another more restrictive condition.

What we want now is that it exists one interval $[\tilde{\sigma}_1, \tilde{\sigma}_2] \subset [0, \sigma_{max}]$ such as

$$\forall \sigma \in [\tilde{\sigma}_1, \tilde{\sigma}_2] \ , \qquad G_\pi(\sigma) \leq \epsilon \ , \tag{30}$$

with $\epsilon \leq 5.10^{-2}$ and $\tilde{\sigma}_1$, $\tilde{\sigma}_2$ as zeroes of $G_\pi(\sigma)$.

If (30) is verified, it is sufficient to take as an optimal CFL number

$$\sigma^* = \begin{cases} e^{-1}\,\tilde{\sigma}_i \ , \quad i = 1,2 & \text{if } \tilde{\sigma}_i \leq \sigma_{max} \ , \\ \sigma_{max} & \text{otherwise.} \end{cases}$$

Among all the experimented values, the optimal RK4 coefficients α_k used in 2–D multigrid context respectively for the spatial approximations $(\mathbf{D_1})$ and $(\mathbf{D_2})$ (that respectively correspond to $(\mathcal{D}_\mathbf{1})$ and $(\mathcal{D}_\mathbf{2})$) have the same values

$$\alpha_1 = 0.11, \ \alpha_2 = 0.2766\ldots, \ \alpha_3 = 0.5, \ \alpha_4 = 1 \ .$$

The curves of the function

$$G_\pi : \ \sigma \in [0, \sigma_{max}] \rightarrow G(\sigma, \pi, \alpha_1, \alpha_2)$$

are represented by the figures 21 and 22. They are the same except they have different maximal values for the CFL.

For the spatial approximation $(\mathcal{D}_\mathbf{1})$, we take

$$\sigma^{1^*} = \sqrt{2}\,\tilde{\sigma}_1^1 \ , \text{ since } \quad \sqrt{2}\,\tilde{\sigma}_2^1 > \sigma_{max}^1 \ ,$$

and if we choose the spatial approximation $(\mathcal{D}_\mathbf{2})$

$$\sigma^{2^*} = \sigma_{max}^2 \ , \text{ since } \quad \sqrt{2}\,\tilde{\sigma}_j^2 > \sigma_{max}^2 \ , \quad j = 1 \text{ or } 2 \ .$$

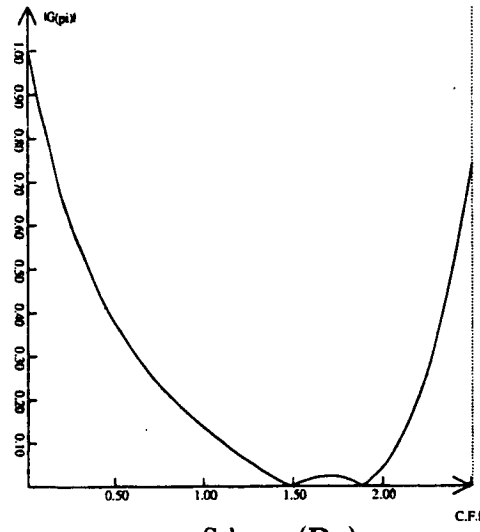

Scheme $(\mathbf{D_1})$

$\sigma^1_{max} = 2.5105$, $\widetilde{\sigma}^1_1 = 1.4869$, $\widetilde{\sigma}^1_2 = 1.8921$

$\alpha_1 = 0.11$, $\alpha_2 = 0.2766$, $\alpha_3 = 0.5$, $\alpha_4 = 1.0$

Figure 21: Curve of the function G_π : $\sigma \in [0, \sigma_{max}] \longrightarrow G(\sigma, \pi, \alpha_1, \alpha_2)$.

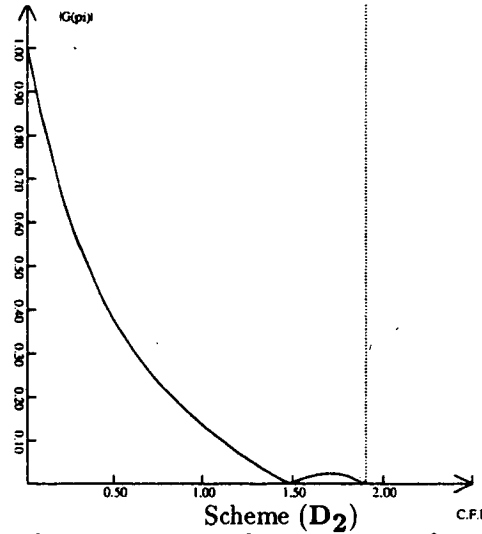

Scheme $(\mathbf{D_2})$

$\sigma^2_{max} = 1.9185$, $\widetilde{\sigma}^2_1 = 1.4869$, $\widetilde{\sigma}^2_2 = 1.8921$

$\alpha_1 = 0.11$, $\alpha_2 = 0.2766$, $\alpha_3 = 0.5$, $\alpha_4 = 1.0$

Figure 22: Curve of the function G_π : $\sigma \in [0, \sigma_{max}] \longrightarrow G(\sigma, \pi, \alpha_1, \alpha_2)$.

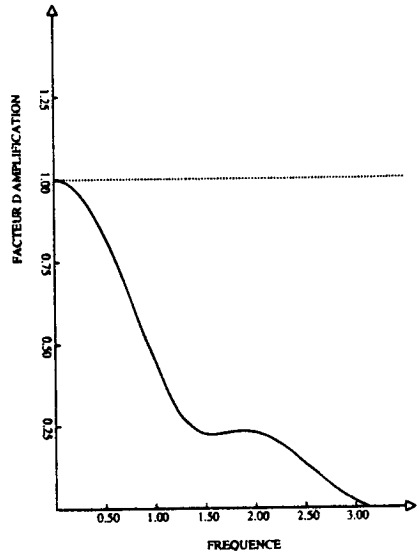

$$\sigma = \widetilde{\sigma}_1^1 = 1.4869.$$
$$\alpha_1 = 0.11\ , \quad \alpha_2 = 0.2766\ , \quad \alpha_3 = 0.5\ , \quad \alpha_4 = 1.0$$

Figure 23: Curve of the amplification factor $\theta \in [0, \pi] \longrightarrow G(\sigma, \theta, \alpha_1, \alpha_2)$

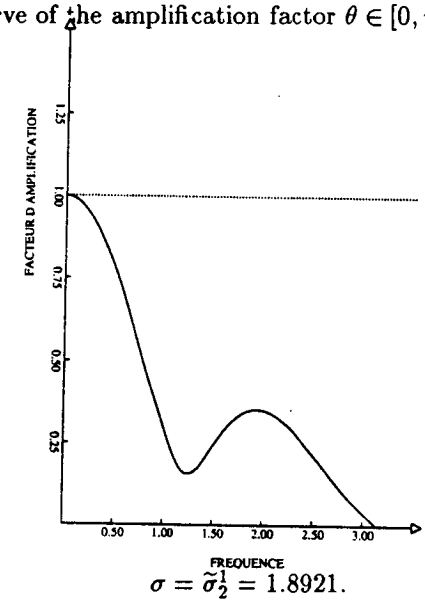

$$\sigma = \widetilde{\sigma}_2^1 = 1.8921.$$
$$\alpha_1 = 0.11\ , \quad \alpha_2 = 0.2766\ , \quad \alpha_3 = 0.5\ , \quad \alpha_4 = 1.0$$

Figure 24: Curve of the amplification factor $\theta \in [0, \pi] \longrightarrow G(\sigma, \theta, \alpha_1, \alpha_2)$

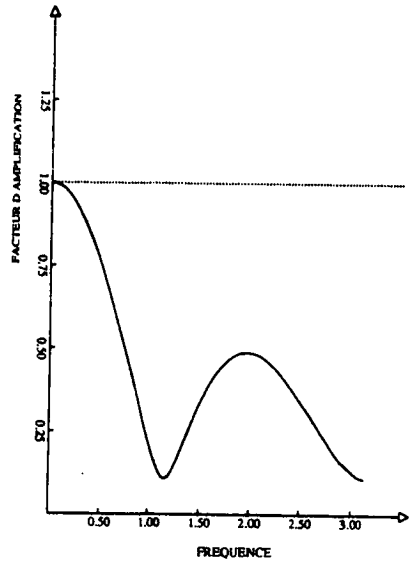

$$\sigma = e^{-1}\,\widetilde{\sigma}_1^1 = 2.1028\,, \quad e = \frac{\sqrt{2}}{2}.$$
$$\alpha_1 = 0.11\,, \quad \alpha_2 = 0.2766\,, \quad \alpha_3 = 0.5\,, \quad \alpha_4 = 1.0$$

Figure 25: Curve of the amplification factor $\theta \in [0,\pi] \longrightarrow G(\sigma,\theta,\alpha_1,\alpha_2)$

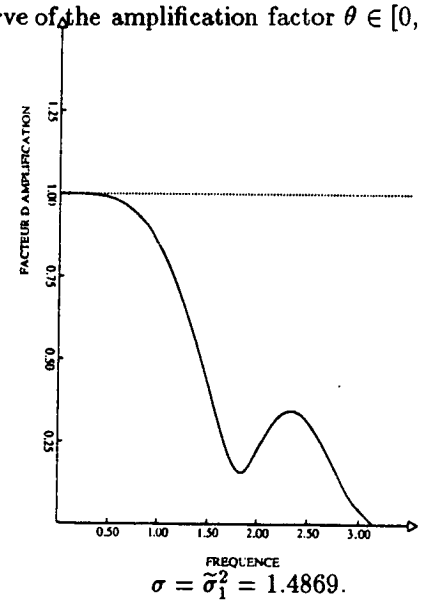

$$\sigma = \widetilde{\sigma}_1^2 = 1.4869.$$
$$\alpha_1 = 0.11\,, \quad \alpha_2 = 0.2766\,, \quad \alpha_3 = 0.5\,, \quad \alpha_4 = 1.0$$

Figure 26: Curve of the amplification factor $\theta \in [0,\pi] \longrightarrow G(\sigma,\theta,\alpha_1,\alpha_2)$

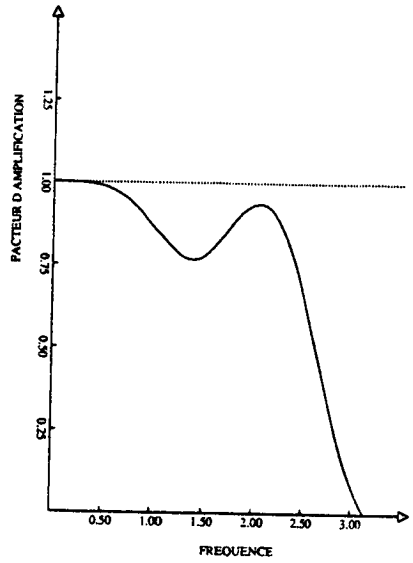

$\sigma = \widetilde{\sigma}_2^2 = 1.8921.$

$\alpha_1 = 0.11\ ,\quad \alpha_2 = 0.2766\ ,\quad \alpha_3 = 0.5\ ,\quad \alpha_4 = 1.0$

Figure 27: Curve of the amplification factor $\theta \in [0, \pi] \longrightarrow G(\sigma, \theta, \alpha_1, \alpha_2)$

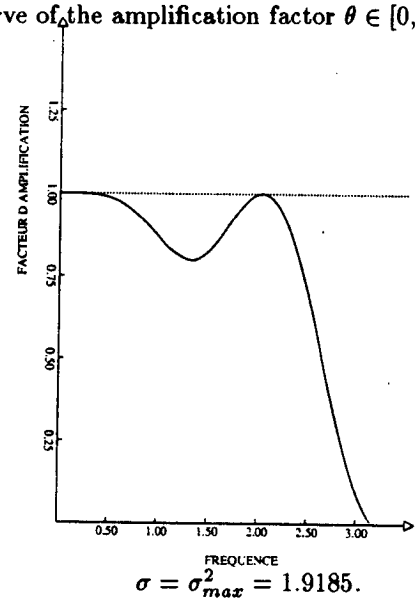

$\sigma = \sigma_{max}^2 = 1.9185.$

$\alpha_1 = 0.11\ ,\quad \alpha_2 = 0.2766\ ,\quad \alpha_3 = 0.5\ ,\quad \alpha_4 = 1.0$

Figure 28: Curve of the amplification factor $\theta \in [0, \pi] \longrightarrow G(\sigma, \theta, \alpha_1, \alpha_2)$

For $(\mathbf{D_1})$, we can see in the figures 23 to 25 the curves of the amplification factor for varying frequencies $\theta \in [0, \pi]$ for the different values $\tilde{\sigma}_1^1$, $\tilde{\sigma}_2^1$, $\sigma^{1\,*}$; for $(\mathbf{D_2})$, the corresponding curves are shown in figures 26 to 28 for $\tilde{\sigma}_1^2$, $\tilde{\sigma}_2^2$, and $\sigma^{2*} = \sigma_{max}^2$.

We have now to validate numerically the results obtained by the previous analysis. As an application, we shall present some computations of the 2–D solution of the Euler equations.

4 NUMERICAL RESULTS

To validate the previous study, two types of computations are done

- 1-grid computations related to the 2–D criterion $[\mathbf{C_1}]$,
- multigrid computations related to the 2–D criterion $[\mathbf{C_2}]$.

1–grid computations

We make a comparison between a numerical test using the standard RK4 scheme, and one using the RK4 scheme optimized according to the criterion $[\mathbf{C_1}]$, for both spatial approximations $(\mathcal{D}_\mathbf{1})$ and $(\mathcal{D}_\mathbf{2})$.

Numerical results related to $(\mathcal{D}_\mathbf{1})$

For the approximation $(\mathcal{D}_\mathbf{1})$, we consider as a model problem an internal transonic flow in a channel with a 4.5% circular bump. The free stream Mach number is 0.85 . The mesh used for this computation is presented in Figure 29 and has 585 nodes and 1056 elements. For the standard RK4 scheme the CFL number has the following value

$$\sigma_s^1 = 1.3926 \ ,$$

which corresponds to the maximal value allowed to preserve the linear stability.

The "optimal" RK4 scheme obtained by the 2–D criterion $[\mathbf{C_1}]$ is defined by the following coefficients

$$\alpha_1 = 0.10,\ \alpha_2 = 0.26,\ \alpha_3 = 0.5,\ \alpha_4 = 1.0,\ \sigma_{opt}^1 = 2.6756 \ ,$$

where σ_{opt}^1 is the maximal value allowed to preserve the (linear) stability of the full scheme.

The convergence histories are shown on Figure 30; where the normalized residual (each residual being divided by its initial value) of the first component of the approximate solution W (i.e. ρ) is plotted versus the number of iterations. Each iteration consists in four calculations of the numerical fluxes (RK4 residual).

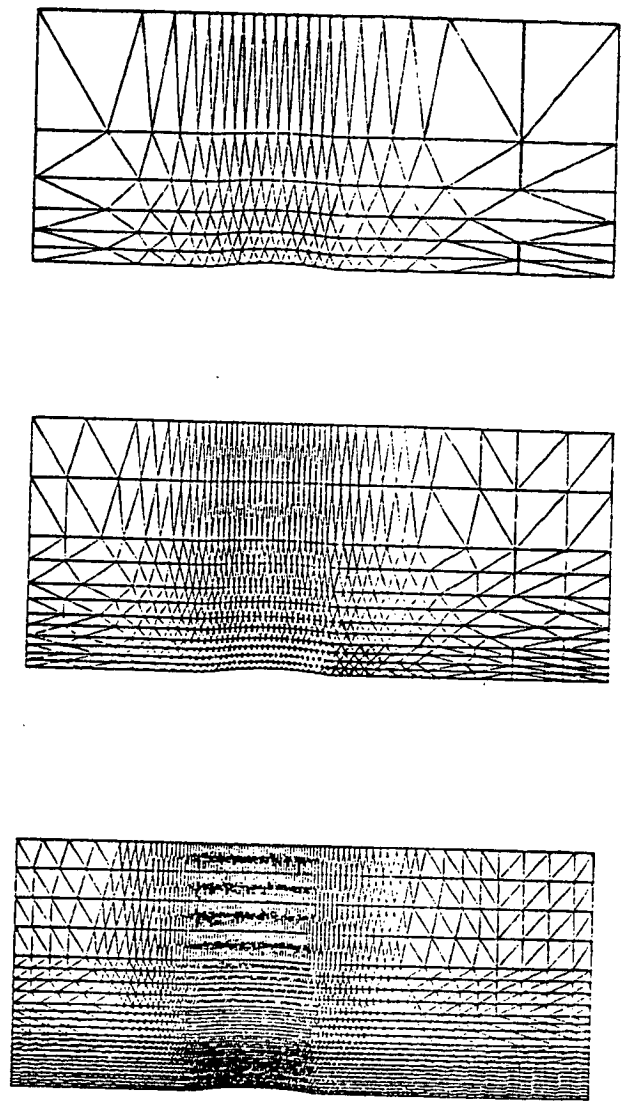

Figure 29: The three level triangulations.

Channel with a circular bump.

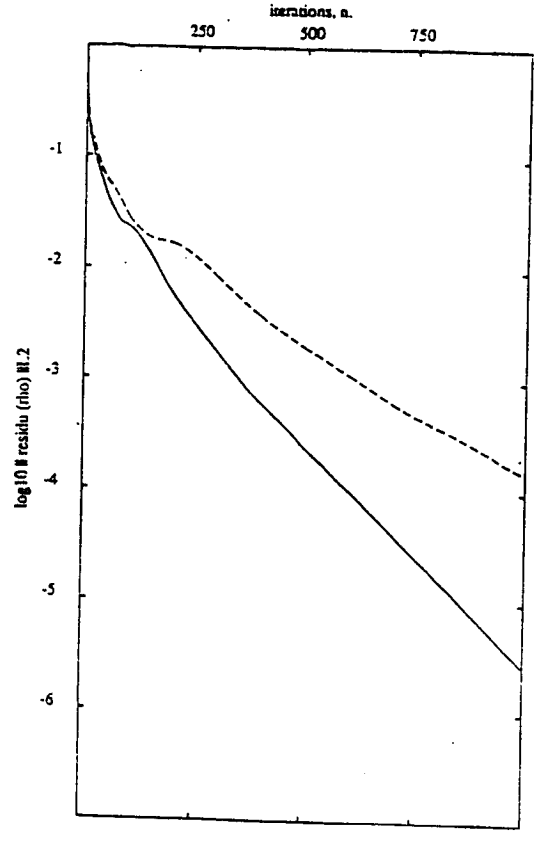

——— $\alpha_1 = 0.10\,,\quad \alpha_2 = 0.26\,,\quad \alpha_3 = 0.5\,,\quad \alpha_4 = 1.\,,\quad \sigma^1_{opt} = 2.6756$

– – – – $\alpha_1 = 0.25\,,\quad \alpha_2 = 0.33\,,\quad \alpha_3 = 0.5\,,\quad \alpha_4 = 1.\,,\quad \sigma^1_s = 1.3926$

Figure 30: Channel with a circular bump (585 nodes). 1–Grid Convergence history. Mach=0.85, spatial approximation ($\mathcal{D}_1$).

The two average reductions of $d\rho/dt$ per iteration denoted by a_s^1 (for the standard RK4 scheme) and by a_{opt}^1 (for the optimized one) for 1000 iterations are

$$\begin{aligned} a_s^1 &= 0.9912 , \\ a_{opt}^1 &= 0.9872 . \end{aligned}$$

For first order accurate spatial approximations it is classical to consider that the steady state is reached when the initial residual is divided by a factor of 10^3. The two convergence histories show that we have a factor of 1.8 between the standard RK4 convergence rate and the optimized one and this factor asymptotically increases. Because the cost of one iteration is the same for both schemes, we thus obtain a gain in efficiency of about 2. for the optimized RK4 scheme.

Numerical results related to $(\mathcal{D}_2)$

For the second order accurate spatial approximation, we choose the classical problem of an external subsonic flow about a NACA0012 airfoil, with a free stream Mach number of 0.72 and 0. degree as an angle of attack. The employed mesh has 442 nodes and 800 elements (see figure 31). For the standard RK4 scheme, we have the following maximal value of the CFL number

$$\sigma_s^2 = 1.3846 .$$

For the "optimal" RK4 scheme (2-D criterion $[\mathbf{C_1}]$) the values of the different parameters are

$$\alpha_1 = 0.12,\ \alpha_2 = 0.26,\ \alpha_3 = 0.5,\ \alpha_4 = 1.0,\ \sigma_{opt}^2 = 2.0763 ,$$

where σ_{opt}^2 is the maximal value of the CFL number.

The convergence histories are shown in the figure 32. The two average reduction factors a_s^2 and a_{opt}^2 respectively evaluated for 655 and 960 iterations are

$$\begin{aligned} a_s^2 &= 0.9865 , \\ a_{opt}^2 &= 0.9800 . \end{aligned}$$

For second order accurate spatial approximations, it is usual to say the steady state is reached when the initial residual is divided by a factor of 10^4. Here the ratio of the convergence rates is only 1.4, but we can notice that it becomes asymptotically greater than 1.5. We thus have a gain in efficiency of about 1.5 for the optimized RK4 scheme.

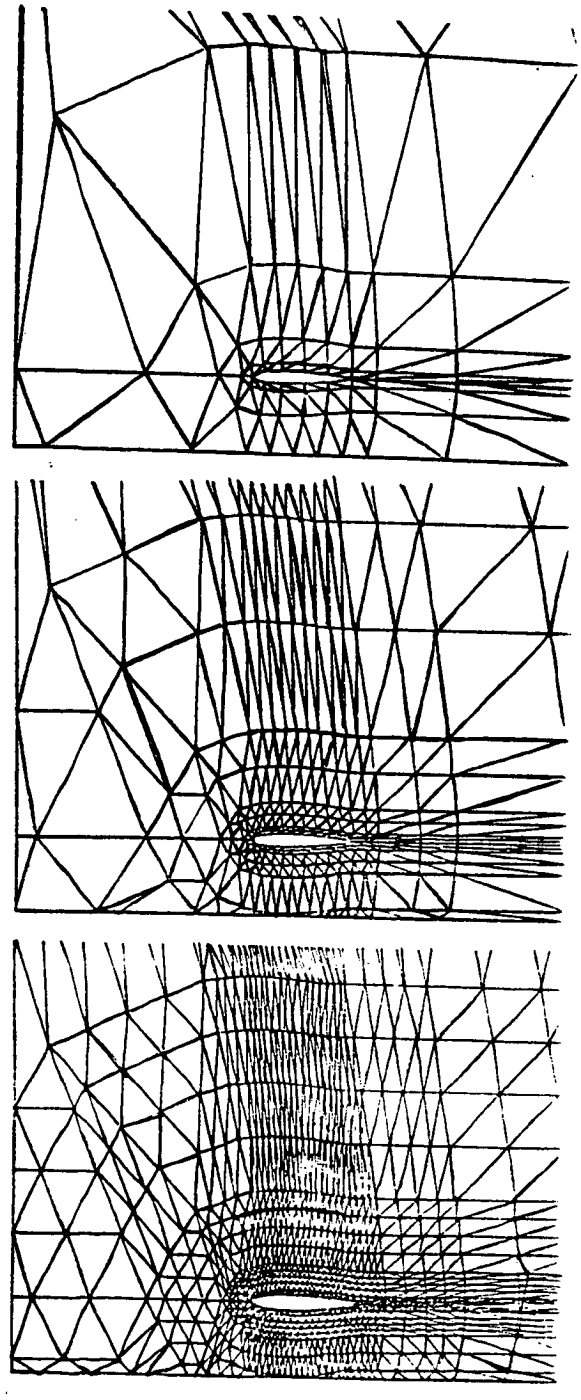

Figure 31: The three level triangulations.

External flow around a NACA0012.

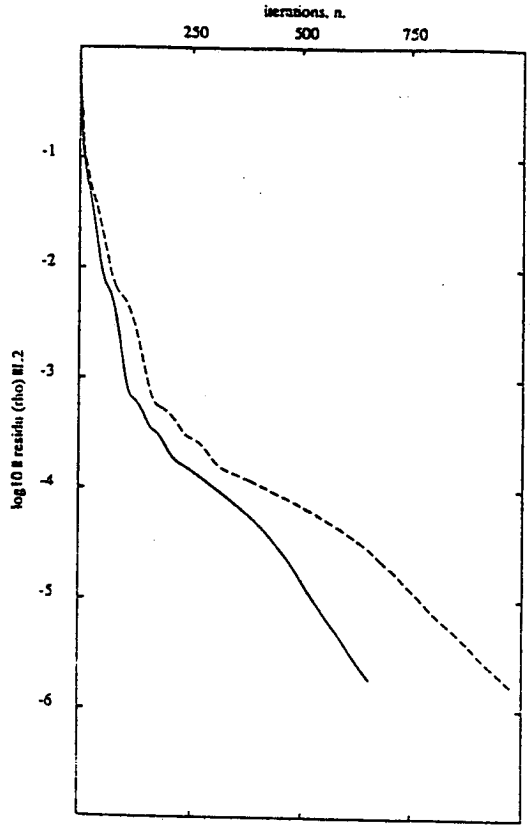

——— $\alpha_1 = 0.12\,,\quad \alpha_2 = 0.26\,,\quad \alpha_3 = 0.5\,,\quad \alpha_4 = 1.0\,,\quad \sigma^2_{opt} = 2.0763$

– – – – $\alpha_1 = 0.25\,,\quad \alpha_2 = 0.33\,,\quad \alpha_3 = 0.5\,,\quad \alpha_4 = 1.0\,,\quad \sigma^2_{s} = 1.3846$

Figure 32: External flow around a NACA0012 (442 nodes). 1–Grid Convergence histories. Mach=0.72, scheme ($\mathcal{D}_2$).

Multigrid numerical results

Numerical results related to $(\mathcal{D}_1)$

We present two 3-Grid numerical results. The test problem is the same as in 4 but the employed fine mesh is finer (it contains 2225 nodes, see figure 29 for the three levels).

The solution method is the basic 3–Grid algorithm. The initial approximate solution at time $t = 0$ is the initial uniform flow given on the finest level (2225 nodes). The "final" steady state solution is the approximate converged solution on the finest level.

We make a comparison between

- a numerical 3–Grid result using the following RK4 scheme

$$\begin{cases} \alpha_1 = 0.11,\ \alpha_2 = 0.2766\ldots,\ \alpha_3 = 0.5,\ \alpha_4 = 1.0\ , \\ \text{with}\quad \sigma^1_{max} = 2.5105\ . \end{cases}$$

- and another one using the same RK4 coefficients α_k but with the following value of the CFL number

$$\sigma^1_{opt} = 2.102807\ .$$

The second scheme is the optimal RK4 scheme i.e. it results from the 2–D multigrid criterion $[\mathbf{C_2}]$.

The two convergence histories are given in the figure 33. The pseudo–unsteady phase of the search is quite perturbed for the first scheme. We can notice that there is a kind of plateau just under the limit 10^{-2}: the algorithm does not converge. This can be explained by the use of a too large CFL number that causes non linear instabilities even if linear stability criterion is respected, and/or by the absence of sufficiently dissipative properties at the maximal value of the CFL.

For the second scheme the asymptotic slope is quickly attained and is smoother.

The average reduction factor of the residual a_{opt} related to the second computation has a value of about 0.9747 for 541 cycles.

Numerical results related to $(\mathcal{D}_2)$

The test problem is the same as in 4, but with a free stream Mach number of 0.85 (transonic flow) and an angle of attack of 1.0 degree. The finest level triangulation contains 1684 nodes and is shown on Figure 31.

We make a comparison between

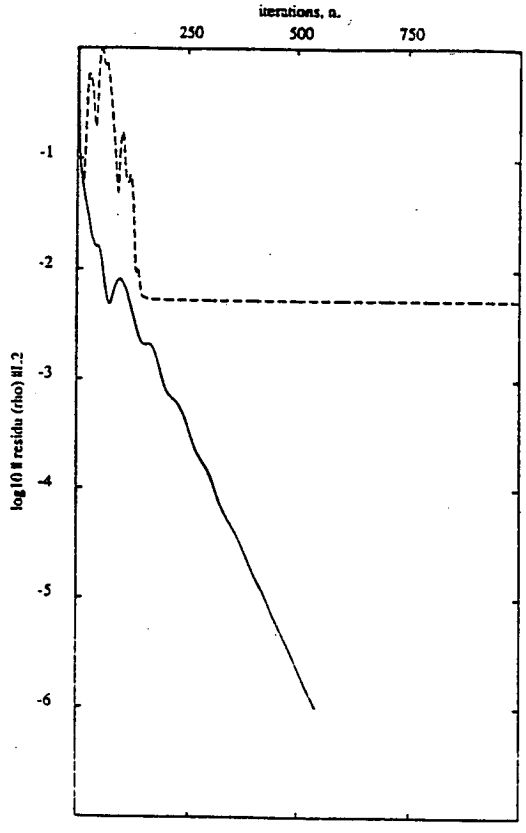

——— $\alpha_1 = 0.11\,,\quad \alpha_2 = 0.2766\,,\quad \alpha_3 = 0.5\,,\quad \alpha_4 = 1.0\,,\quad \sigma^1_{opt} = 2.1028$

– – – – $\alpha_1 = 0.11\,,\quad \alpha_2 = 0.2766\,,\quad \alpha_3 = 0.5\,,\quad \alpha_4 = 1.0\,,\quad \sigma^1_{max} = 2.5105$

Figure 33: Channel with a circular bump (2225 nodes). 3–Grid Convergence histories. Mach=0.85, scheme ($\mathcal{D}_1$).

- a 3–Grid numerical result (basic multigrid algorithm) using the following optimized RK4 scheme (i.e. resulting from the criterion $[\mathbf{C_2}]$)

$$\begin{cases} \alpha_1 = 0.11,\ \alpha_2 = 0.2766\ldots,\ \alpha_3 = 0.5,\ \alpha_4 = 1.0\ , \\ \text{with}\quad \sigma^2_{opt} = 1.9185\ . \end{cases}$$

  The value of the CFL number σ^2_{opt} is the maximal value allowed to preserve the stability of the full scheme, but in this case it also has good dissipative properties.

- a 1–Grid numerical result on the finest grid using the optimal RK4 scheme i.e. that satisfies the criterion $[\mathbf{C_1}]$ whose coefficients are

$$\begin{cases} \alpha_1 = 0.12,\ \alpha_2 = 0.26,\ \alpha_3 = 0.5,\ \alpha_4 = 1.0\ , \\ \text{with}\quad \sigma^2_{max} = 2.0763\ . \end{cases}$$

We give in Figure 34, the two corresponding convergence histories. The two average reduction factors a_{3G} and a_{1G} evaluated respectively for 507 3–Grid cycles and 1000 1–Grid iterations are

$$\begin{aligned} a_{3G} &= 0.9730\ , \\ a_{1G} &= 0.9902\ . \end{aligned}$$

3–Grid cycle cost

Let C_k be the cost of one numerical flux on the grid $G_k \quad k = 1, 2, 3$, the index 3 corresponding to the index of the finest grid.

We can assume that $C_{k+1} \simeq 4\,C_k$, because the ratio between the number of nodes of two successive grids (fine–coarse) is about 4. Denote by C_{3G} the cost of one 3–Grid cycle, then we have

$$\begin{aligned} C_{3G} &= 4\,C_3 + C_3 + 3\,C_2 + C_2 + 3\,C_1\ , \\ &= C_3\,(6 + \frac{3}{16}) \simeq 6.2\,C_3\ . \end{aligned} \tag{31}$$

Factors of 3 (and not 4) appear in front of C_2 and C_1; this is because, in the first step of the RK4 method, the current level RK4 residual is reduced to a simple transfer of the previous finer level source term (see [11], chapter 1) in the implementation of the algorithm; hence the current level numerical flux need not be evaluated in this first step. However, if this assumption is not made,

$$\begin{aligned} C_{3G} &= 4\,C_3 + C_3 + C_2 + 4\,C_2 + C_2 + C_1 + 4\,C_1\ , \\ &= C_3\,(5 + \frac{6}{4} + \frac{5}{16}) \simeq 6.8\,C_3\ . \end{aligned} \tag{32}$$

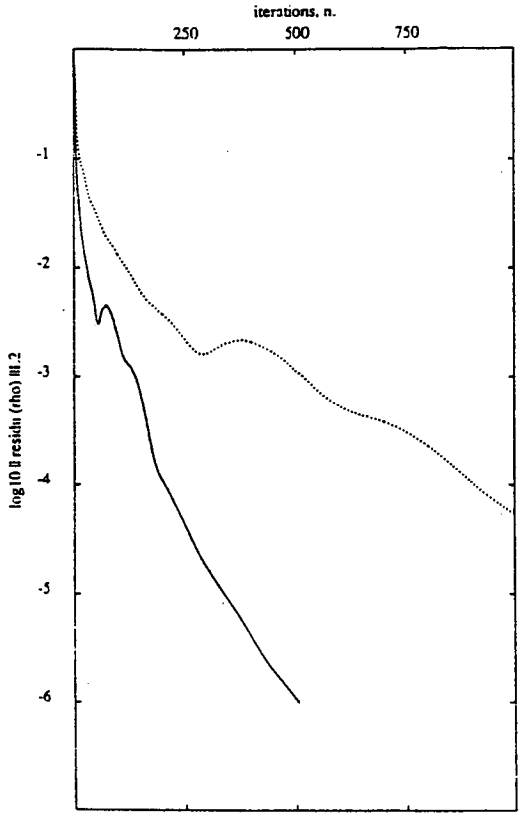

——— $\alpha_1 = 0.11\,,\quad \alpha_2 = 0.2766\,,\quad \alpha_3 = 0.5\,,\quad \alpha_4 = 1.0\,,\quad \sigma^2_{opt} = 1.9185$

····· $\alpha_1 = 0.12\,,\quad \alpha_2 = 0.26\,,\quad \alpha_3 = 0.5\,,\quad \alpha_4 = 1.0\,,\quad \sigma^2_{max} = 2.0763$

Figure 34: NACA0012 airfoil (1684 nodes). 1–Grid and 3–Grid Convergence histories. Mach=0.85, angle of attack = 1.0 deg., scheme ($\mathcal{D}_2$).

Since one 1–Grid iteration on G_3 is about $4\,C_3$, we can deduce that one 3–Grid cycle is about 1.55 (if evaluated by (31)), or 1.7 (if evaluated by (32)), times 1–Grid iterations on G_3.

As the ratio of the convergence rates (evaluated when the initial residual is divided by a factor of 10^4) is about 4.5, we can conclude that the 3–Grid algorithm is 2.5 times more efficient than the 1–Grid algorithm on grid G_3.

CONCLUSION

We have presented a simple method to optimize a 4 steps Runge–Kutta scheme combined to first or second order accurate upwind spatial approximations of the 2–D Euler equations. This optimization is carried with particular attention to situations where unstructured finite element discretizations are employed in the multigrid context.

First the optimization is done on a 1–D classical linear model problem. The optimized RK4 scheme is deduced from selecting the different parameters (the RK4 coefficients and the Courant number), according to some appropriate criteria. These criteria are different for the 1–Grid and multigrid strategy.

In the 1–Grid context, the criterion is essentially based on the largest stability domain we can obtain; we indeed want to use large time steps i.e. we want to have a large convergence rate.

In the multigrid context, we have to consider another criterion based on the dissipative (smoothing) properties that the basic solver scheme should have. More precisely, we have to determine the different coefficients so as to damp the highest frequency components of the error. We recall that the damping of low frequency components is realized by the transfer of the discrete problem to a coarser grid. The present approach is simplified because the optimization is only done for the highest frequency $\theta = \pi$ and not for all the frequencies lying in $[\pi/2, \pi]$; however, a more complete analysis is presented in appendix where we check a posteriori the validity of the present simplified analysis.

In a "second round", we try to extend the previous ideas to the 2–D unstructured finite element discretizations context. This is done according to geometrical criteria, in which the principles developed in the previous 1–D analysis are slightly modified.

The numerical results presented here and in [11, 12] allow us to assert that the present theoretical study permits to choose an efficient multigrid algorithm.

5 APPENDIX

We add a numerical result as a justification a posteriori of the validation of the previous study results.

As a more complete (and classical) approach, we optimize now the coefficients α_1, α_2 et σ as a solution of the following Min–Max problem (straightforward 2–D extension)

$$\min_{\substack{\alpha_1,\alpha_2\in]0,1] \\ \sigma>0}} \max_{(\theta_1,\theta_2)\in P} |G(\sigma,\theta_1,\theta_2,\alpha_1,\alpha_2)| \ ,$$

where $P = P_1 \cup P_2 \cup P_3$ is the set of all high frequencies, with

$$\begin{aligned}
P_1 &= \left\{(\theta_1,\theta_2) \ ; \ 0 \le \theta_1 \le \frac{\pi}{2} \ , \ \frac{\pi}{2} \le \theta_2 \le \pi\right\} \ , \\
P_2 &= \left\{(\theta_1,\theta_2) \ ; \ \frac{\pi}{2} \le \theta_1 \le \pi \ , \ 0 \le \theta_2 \le \frac{\pi}{2}\right\} \ , \\
P_3 &= \left\{(\theta_1,\theta_2) \ ; \ \frac{\pi}{2} \le \theta_1 \le \pi \ , \ \frac{\pi}{2} \le \theta_2 \le \pi\right\} \ , \\
P_4 &= \left\{(\theta_1,\theta_2) \ ; \ 0 \le \theta_1 \le \frac{\pi}{2} \ , \ 0 \le \theta_2 \le \frac{\pi}{2}\right\} \ ,
\end{aligned}$$

P_4 corresponds to the set of the low frequencies.

Solving this problem is to optimize the maximal value of the amplification factor only for the high frequencies. We thus optimize the RK4 "smoother".

Moreover, the value of the Courant number σ has to verify the stability condition

$$\max_{(\theta_1,\theta_2)\in P\cup P_4} |G(\sigma,\theta_1,\theta_2,\alpha_1,\alpha_2)| \le 1 \ .$$

A software researching the optima, and based on the discretized problem, allows us to determine the following values concerning the spatial approximation $(\mathcal{D}_2)$

$$\alpha_1 = 0.1198 \ , \quad \alpha_2 = 0.2728 \ , \quad \alpha_3 = 0.5 \quad \alpha_4 = 1.0 \ , \quad \sigma = 0.905 \ , \qquad (33)$$

that can be distinguished from those previously found by the more reduced allowable time step since

$$\alpha_1 = 0.11 \ , \quad \alpha_2 = 0.2766 \ , \quad \alpha_3 = 0.5 \ , \quad \alpha_4 = 1.0 \ , \quad \sigma = 1.9185 \ . \qquad (34)$$

The test problem is the one described in § 4.1 for the spatial scheme $(\mathcal{D}_2)$, when using the 3–Grid algorithm. The fine grid we use contains 1684 nodes (cf. figure 31).

The convergence histories are given in the figure 35. For a tolerance fixed to 10^{-4} (the initial residual is divided by four decades), we thus obtain a gain in efficiency and in convergence rate of about 2 (1.875), this gain becomes more than 2 (2.102) for a tolerance of 10^{-6}. Because both RK4 coefficients (except the time step) are quite the same, we can notice that the size of the allowable time step is very important and has to be taken into account so as to get an efficient multigrid method in the hyperbolic context.

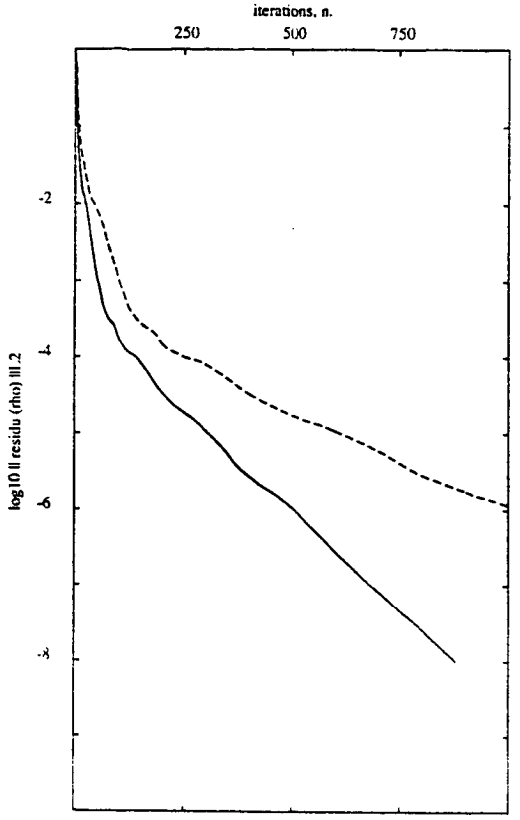

——— $\alpha_1 = 0.11$, $\alpha_2 = 0.2766$, $\alpha_3 = 0.5$, $\alpha_4 = 1.0$, $\sigma = 1.9185$

– – – – $\alpha_1 = 0.1198$, $\alpha_2 = 0.2728$, $\alpha_3 = 0.5$, $\alpha_4 = 1.0$, $\sigma = 0.905$

Figure 35: NACA0012 airfoil (1684 nodes). 3-Grid Convergence histories. Mach = 0.72, scheme ($\mathcal{D}_2$).

Although the scheme defined by (33) has best smoothing properties (for the damping of high frequencies, see figure 36 for (33), figure 28 for (34)), the too small value taken by σ make the multigrid convergence rate decrease. That can appear as a contradiction according to the classical multigrid theory for elliptic problems upon the smoother; but we are concerned with hyperbolic problems and thus we have to account for the convection phenomena (wave propagation) that cannot be under estimated.

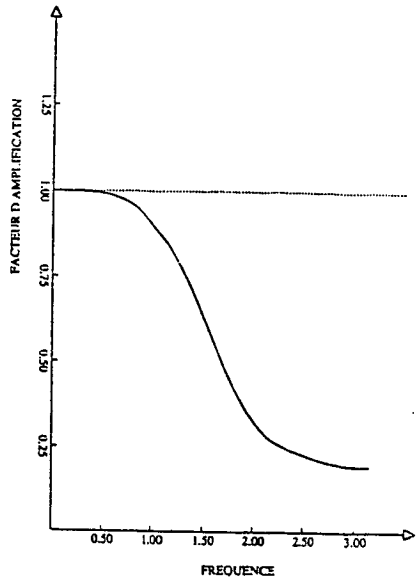

$\alpha_1 = 0.1198$, $\alpha_2 = 0.2728$, $\alpha_3 = 0.5$, $\alpha_4 = 1.0$
$\sigma = 0.905$ (schéma $(\mathcal{D}_2)$).

Figure 36: Curve of the amplification factor $\theta \in [0, \pi] \longrightarrow G(\sigma, \theta, \alpha_1, \alpha_2)$

References

[1] F. ANGRAND, P. LEYLAND. Schéma multigrille dynamique pour la simulation d'écoulements de fluides visqueux compressibles, *Rapport de Recherche INRIA*, No. 659, avril 1987.

[2] P. BALLARD, *Rapport de stage effectué aux AMD-BA*, Ecole Polytechnique option B2, 1987.

[3] A. BRANDT. Multigrid techniques: 1984 Guide with Applications to Fluid Dynamics, *G.M.D-Studien*, No. 85, May 1984.

[4] A. DERVIEUX. Steady Euler Simulations using unstructured meshes, *Cours Von Karman Institute for Fluid Dynamics*, Lecture series 1985–04, (1985), publié dans *Partial Differential Equations of Hyperbolic Type and Applications*, G. Geymonat (Ed.), World Scientific, 1987.

[5] J-A. DESIDERI, A. GOUDJO, V. SELMIN. Third-order numerical schemes for hyperbolic problems, *Rapport de Recherche INRIA*, No. 607, février 1987.

[6] F. FEZOUI. Résolution des Equations d'Euler par un Schéma de van Leer en Eléments Finis, *Rapport de Recherche INRIA*, No. 358, janvier 1985.

[7] A. HARTEN, P.D. LAX, B. VAN LEER. On Upstream Differencing and Godunov Type Schemes for Hyperbolic Conservation Laws, *SIAM Review*, **25** (1), 1983.

[8] A. JAMESON. Numerical solution of the Euler equations for compressible inviscid fluids, in *Numerical methods for the Euler equations of Fluid Dynamics*, F.Angrand et al. (eds.), SIAM, Philadelphia, 1985.

[9] A. JAMESON. The evolution of Computational methods in aerodynamics, *MAE* Report No. 1608, May 1983.

[10] A. JAMESON. Multigrid Algorithms For Compressible Flow Calculations, *MAE* Report No. 1743, October 1985.

[11] M-H. LALLEMAND, F. FEZOUI, E. PEREZ, Un Schéma Multigrille en Eléments Finis Décentré pour les Equations d'Euler, *Rapport de recherche INRIA*, No 602, 1987.

[12] M-H. LALLEMAND, Schémas Décentrés Multigrilles pour la Résolution des Equations d'Euler en Eléments Finis, *Thése de Doctorat*, Université de Provence, Marseille, mars 1988.

[13] B. PALMERIO, V. BILLEY, J. PERIAUX, A. DERVIEUX. Self Adaptative Mesh Refinements and Finite Element Methods For Solving the Euler Equations, in *Numerical methods for Fluid Dynamics* II, K.W. Morton, M.I. Baines Eds., Clarendon Press, Oxford 1986.

[14] E. PEREZ. Finite Element and Multigrid solution of the two-dimensional Euler equations on a non-structured mesh, *Rapport de Recherche INRIA* 442, 1985.

[15] E. PEREZ, J. PERIAUX, J-P. ROSENBLUM, B. STOUFFLET, A. DERVIEUX , M-H. LALLEMAND. Adaptive full-multigrid finite element methods for solving the two-dimensional Euler equations, *Proceedings Tenth International Conference on Numerical Methods in Fluid Dynamics*, Beijing (China), June 1986, Lecture Notes in Physics no 254, Springer Verlag.

[16] E. TURKEL, B. VAN LEER. Flux vector splitting and Runge-Kutta methods for the Euler equations, *ICASE* Report 84-27, June 1984.

[17] E. TURKEL. Acceleration to a Steady State for the Euler Equations, in *Numerical methods for the Euler equations of fluid dynamics*, F. Angrand et al. (éd.), SIAM, 1985.

[18] B. VAN LEER. Towards the Ultimate Conservative Difference Scheme III, *Journal of Computational Physics*, **23**, 263-275, 1977.

Imprimé en France
par
l'Institut National de Recherche en Informatique et en Automatique